AN ABSTRACT OF THE THESIS OF

Dmitry A. Smolyansky for the degree of Master of Science in Electrical and Computer Engineering presented on September 30, 1994.

Title: Enhanced Accuracy Time Domain Reflection and Transmission Measurements for IC Interconnect Characterization

Redacted for Privacy

Abstract approved: Dr. Vijai .K. Tripathi

The purpose of this study is to develop accuracy enhancement techniques for the Time Domain Reflection/Transmission (TDR/T) measurements including the analysis of the error sources for the Enhanced Accuracy TDR/T (EA-TDR/T). These TDR/T techniques are used for IC and IC package interconnect characterization and equivalent circuit model extraction, which are important for evaluating the overall system performance in today's digital IC design.

The frequency domain error correction has been used to get parameters for a Device Under Test (DUT) from time domain measurements. The same technique can be used as an intermediate step for obtaining the EA-TDR/T.

Careful choice of the acquisition window and precise alignment of the DUT and calibration standard waveforms are necessary to get the accuracy enhancement for the TDR/T. Improved FFT techniques are used in order to recover the actual spectra of the step-like time domain waveforms acquired with an acquisition window with a finite time length. The EA-TDR/T waveform are recovered from error corrected frequency domain

parameters of the DUT by launching an ideal excitation at the DUT and finding the response. The rise time of the ideal excitation can be faster than that of the physical excitation in the measurement system. However, excessive high-frequency noise can enter the system if the rise time of the ideal excitation is chosen to be too high.

The resulting EA-TDR/T waveforms show significantly less aberrations than the conventional TDR/T waveforms, hence allow us to extract accurate equivalent circuit model for the DUT, which in our case is IC interconnects.

Enhanced Accuracy Time Domain Reflection and Transmission Measurements For IC Interconnect Characterization

by

Dmitry A. Smolyansky

A THESIS

submitted to

Oregon State University

in partial fulfillment of
the requirements of the
degree of

Master of Science

Completed September 30, 1994

Commencement June 1995

APPROVED:

Redacted for Privacy

Professor of Electrical and Computer Engineering in charge of major

Redacted for Privacy

Head of department of Electrical and Computer Engineering

Redacted for Privacy

Dean of Graduate School

Date thesis is presented September 30, 1994

Presented by Dmitry A. Smolyansky

ACKNOWLEDGMENTS

The author is very grateful to his academic advisor, Dr. Vijai K. Tripathi, for his advice, support and understanding.

The author would also like to thank Leonard A. Hayden (N.I.S.T.) and Scott K. Diamond (Tektronix, Inc.) for many fruitful discussions, which helped develop this report.

TABLE OF CONTENTS

LIST OF FIGURES

LIST OF TABLES

ENHANCED ACCURACY TIME DOMAIN REFLECTION AND TRANSMISSION MEASUREMENTS FOR IC INTERCONNECT CHARACTERIZATION

1. INTRODUCTION

As the IC designs become more and more complex and the clock speeds increase rapidly, it is the interconnects that limit the overall performance of the system [1]. Multiple reflections, crosstalk and ground bounce occur, distorting the signal and degrading the signal rise time.

To guarantee the overall system performance, it is necessary to characterize the interconnects and IC packages, simulate the critical signal paths and the interconnect effects [2-3]. The extraction techniques for the equivalent circuit model for the interconnects have been developed in the recent years [4-9]. To get a good starting point for the equivalent circuit model extraction, it is very important that a clean Time Domain Reflection/Transmission (TDR/T) waveform is acquired.

The following report develops a technique for acquiring Enhanced Accuracy TDR/T (EA-TDR) waveforms for the IC interconnects. This technique allows one to obtain a good starting point for accurate interconnect equivalent circuit model extraction.

2. REVIEW OF TIME DOMAIN MEASUREMENT TECHNIQUES

2.1 Time Domain Measurements

2.1.1 Time domain reflection and transmission

Time Domain Reflection and Transmission (TDR/T) measurements are extensively used in the industry as quantitative tools for transmission structure characterization. A block diagram of a typical TDR/T system setup is shown on Fig. 1.

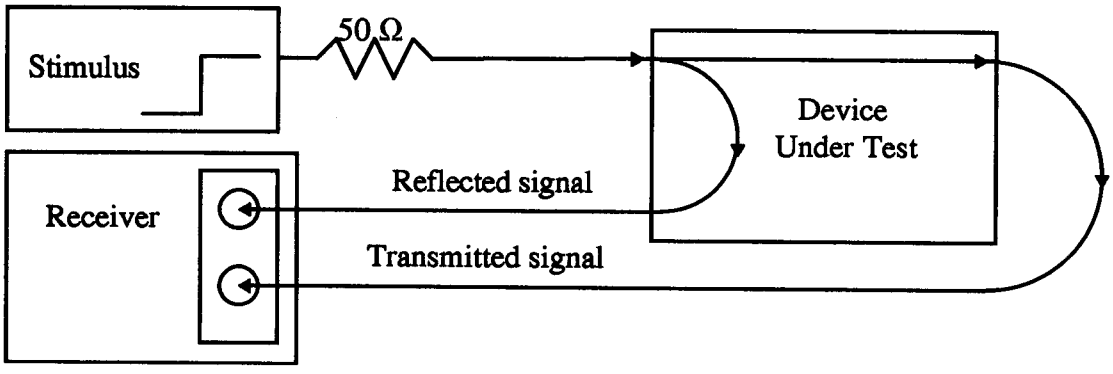

Fig. 1. A block diagram of time domain reflection and transmission measurement system

This measurement system employs a source of a stimulus signal and a receiver. The stimulus signal used in TDR/T measurements is step-like. The receiver allows one to acquire reflection as well as transmission waveforms of the Device Under Test (DUT).

The advantages of TDR/T techniques are their visual nature and intrinsic impedance reference. The broadband character of the stimulus signal allows parallel postprocessing of the acquired data.

With the arrival of high precision digital storage oscilloscopes, TDR has become a tool that allows one to make a qualitative analysis of impedance of the DUT. The impedances have been measured with ±2 Ω accuracy for a 50 Ω reference impedance [10]. The equivalent circuit model then can be extracted from the TDR profile [5,6]. TDT measurements, on the other hand, are important for lossy transmission line characterization. The TDR techniques have been used for wide-band device characterization [11], and faster TDR systems have been developed to improve the measurement system [12].

For a DUT with a complex impedance structure, the TDR/T trace may lose the necessary resolution due to multiple reflections (see Appendix A). The Z-profile algorithm has been developed to deal with this problem [13,14]. This dynamic deconvolution algorithm allows one to get a clean impedance profile for the DUT, minimizing the effect of multiple reflections.

2.1.2 Time domain network analysis

Time domain is where the real events occur and problems originate. However, it s often more convenient to use frequency domain parameters of the DUT for design and analysis purposes. Time Domain Network Analysis (TDNA) allows one to get frequency domain parameters of the DUT using FFT of the TDR/T measurements.

2.2 Calibration Techniques

Frequency domain calibration techniques can be used in order to further increase the precision of the TDNA [15-18]. We will focus on a simple Open-Short-Load (OSL) calibration technique for one port and OSL-Through (OSLT) technique for two port. There are more involved and presumably more accurate calibration methods available [19-21].

2.2.1 One-port calibration

The error model used in the following calibration procedure is described in [15-17] and is illustrated by the signal flow diagram on Fig. 2.

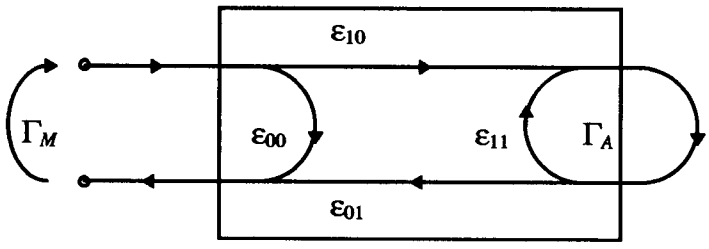

Fig. 2. One-port error model signal flow diagram

The measured reflection coefficient for the DUT is

$$\Gamma_M = \varepsilon_{00} + \frac{\varepsilon_{10}\varepsilon_{01} \cdot \Gamma_A}{1 - \varepsilon_{11} \cdot \Gamma_A} \tag{1}$$

Therefore the actual reflection coefficient can be recovered using equation

$$\Gamma_A = \frac{\Gamma_M - \varepsilon_{00}}{\varepsilon_{11} \cdot (\Gamma_M - \varepsilon_{00}) + \varepsilon_{10}\varepsilon_{01}} \tag{2}$$

where ε_{ij} are found from the OSL calibration procedure (see Appendix B)

2.2.2 Two-port calibration

The flow diagram for the first port of a two port error model [15-17] is shown on Fig. 3.

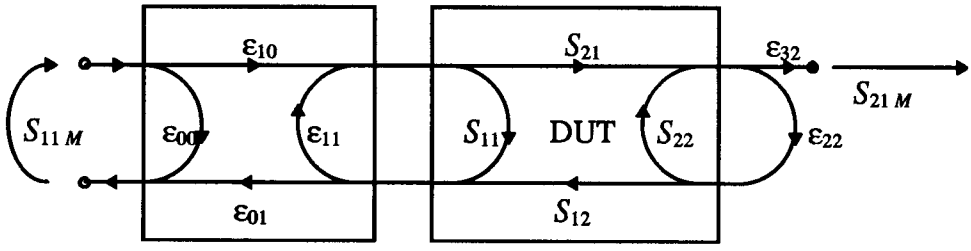

Fig 3. Two-port error model signal flow diagram

The model described by this flow diagram neglects the coupling between the ports. This assumption holds very well for the time domain measurement systems, since the channels in the modern oscilloscopes and sampling heads are physically decoupled.

The measured frequency domain parameters are:

$$S_{11M} = \varepsilon_{00} + (\varepsilon_{10}\varepsilon_{01}) \cdot \frac{S_{11A} - \varepsilon_{22} \cdot \mathrm{Det}(S_A)}{1 - \varepsilon_{11} \cdot S_{11A} - \varepsilon_{22} \cdot S_{22A} + \varepsilon_{11} \cdot \varepsilon_{22} \cdot \mathrm{Det}(S_A)} \tag{3}$$

$$S_{21M} = (\varepsilon_{10}\varepsilon_{32}) \cdot \frac{S_{21A}}{1 - \varepsilon_{11} \cdot S_{11A} - \varepsilon_{22} \cdot S_{22A} + \varepsilon_{11} \cdot \varepsilon_{22} \cdot \mathrm{Det}(S_A)} \tag{4}$$

$$\mathrm{Det}(S_A) = S_{11A} \cdot S_{22A} - S_{21A} \cdot S_{12A} \tag{5}$$

Then the actual frequency domain parameters will be

$$S_{11A} = \frac{\left(\frac{S_{11M} - \varepsilon_{00}}{\varepsilon_{10}\varepsilon_{01}}\right)\left(1 + \frac{S_{22M} - \varepsilon'_{33}}{\varepsilon'_{23}\varepsilon'_{32}} \cdot \varepsilon'_{22}\right) - \varepsilon_{22} \cdot \frac{S_{21M}}{\varepsilon_{10}\varepsilon_{32}} \cdot \frac{S_{12M}}{\varepsilon'_{23}\varepsilon'_{01}}}{D} \tag{6}$$

$$S_{21A} = \frac{\frac{S_{21M}}{\varepsilon_{10}\varepsilon_{32}} \cdot \left[1 + \frac{S_{22M} - \varepsilon'_{33}}{\varepsilon'_{23}\varepsilon'_{32}} \cdot (\varepsilon'_{22} - \varepsilon_{22})\right]}{D} \tag{7}$$

$$D = \left(1 + \frac{S_{11M} - \varepsilon_{00}}{\varepsilon_{10}\varepsilon_{01}} \cdot \varepsilon_{11}\right)\left(1 + \frac{S_{22M} - \varepsilon'_{33}}{\varepsilon'_{23}\varepsilon'_{32}} \cdot \varepsilon'_{22}\right) - \frac{S_{21M}}{\varepsilon_{10}\varepsilon_{32}} \cdot \frac{S_{12M}}{\varepsilon'_{23}\varepsilon'_{01}} \cdot \varepsilon_{22} \cdot \varepsilon'_{11} \tag{8}$$

The parameters with a prime sign (ε'_{ij}) correspond to the second port error model, which is reciprocal for the first port model. The correspondence between the first and second port parameters is shown in Table 1.

Table 1. Notations for the second port parameters and their correspondence to the first port parameters

1st port	ε_{00}	ε_{11}	$\varepsilon_{10}\varepsilon_{01}$	ε_{22}	ε_{32}	$\varepsilon_{10}\varepsilon_{32}$
2nd port	ε'_{33}	ε'_{22}	$\varepsilon'_{23}\varepsilon'_{32}$	ε'_{11}	ε'_{01}	$\varepsilon'_{01}\varepsilon'_{23}$

2.3 Errors in the Measurement System

The sources of errors in the TDR/T measurement system employing the frequency domain calibration have been identified in [22-27]. They are:

A. Hardware errors

1. vertical (voltage or impedance) scale errors, such as

a) noise floor

b) quantization error

c) nonlinearity, gain and offset of the DSO vertical scale

2. horizontal (time base) scale errors, such as

a) time jitter, causing phase errors in frequency domain

b) temperature time base drift – long and short term

c) nonlinearity of the time base

3. nonrepeatability of the measurement due to the mechanical breaking and restoring of the connection at the DUT reference plane, and flexing of the connecting cables

B. Signal processing errors

1. aliasing due to undersampling of the signal

2. truncation errors, caused by the portion of the waveform left out of the measurement window

The repeatable residual signals in the system constitute an error as well, but we correct for them using the frequency domain calibration procedure.

3. ENHANCED ACCURACY TDR/T (EA-TDR/T)

The error correction procedures used for frequency domain vector network analysis measurements can also be used to get the enhanced accuracy of the TDR/T measurements and are presented below.

3.1 Algorithm for Acquiring EA-TDR/T

The algorithm for acquiring the EA-TDR/T waveforms is as follows:

A. Acquire the waveforms of the DUT and calibration standards.

B. take the FFT of the waveforms using algorithms that ensure the correct interpretation of the data spectrum

C. Calibrate the DUT waveform in frequency domain using OSL calibration procedure for one port or OSLT calibration procedure for two port as described in Section 2.2.

D. Recover the DUT time domain waveforms. The recovered waveforms are the EA-TDR/T ones.

3.2 Data Acquisition

The acquisition window for EA-TDR/T needs to be long enough to include all the transients characterizing the DUT. Otherwise the information about the DUT will not be complete and the truncation errors will occur.

On the other hand, as we will discuss later, a shorter acquisition window will lead to higher effective power of the stimulus signal. This constraint together with the requirement of having all the transients characterizing the DUT inside the acquisition window are the basis for the compromise necessary to find the optimal length for the acquisition window.

The OSL(T) calibration procedure requires acquisition of the DUT waveform as well as several calibration standards waveforms. The waveforms need to be aligned in time very precisely. Even minor time base drift will lead to phase drift in frequency domain and the frequency domain error correction procedure will produce inaccurate results..

To decrease the noise level in our measurements, we can increase the number of averages as well as the number of sampling points in the acquisition window [28]. We will discuss it in more detail later in this report.

3.3 FFT Techniques for Step-Like Waveforms

There are several artifacts introduced in the system by the FFT processing due to the fact that our acquisition window has a finite time length. The FFT processing views our data as periodic [29], with their period being equal to the length of the acquisition window. Therefore the excitation step waveform, for example, is effectively a pulse train from the FFT processing point of view. On the other hand, the start and the end points of the data in the acquisition window are not always the same. This would cause a sharp discontinuity in the data as seen by the FFT processing, manifesting itself in high frequency components which may not have been present in the original signal.

Because of these effects, we can not get the correct spectra of the stimulus, calibration standards and DUT waveforms by applying the conventional FFT to these waveforms. Several techniques have been developed to recover the correct spectra of the step-like waveforms [30-32], but all of them have been shown to be analytically the same [33]. The choice is dependent on reader preferences.

Other algorithms have been reported in recent years [34-38], but none of them change the fundamental approach to taking the FFT of a step-like waveforms: remove the effective discontinuity at the end of the waveform in a physical or analytical manner, take the FFT of the corrected waveform, and then recover the spectrum of the original waveform from the corrected waveform spectrum. Some of these algorithms claim to improve the resolution of the improved FFT. They, however, merely use digital interpolation and zero-padding, which interpolate between the points and do

not recover the additional information about the data. They also share the common problem of the improved FFT waveform – inability to recover the value of the waveform spectrum at zero frequency (DC value).

3.3.1 Samulon method

We chose the Samulon algorithm [30] to take the improved FFT of the data. The first step in this algorithm is to take the finite difference of the data and FFT the obtained waveform. Then the spectrum of the original waveform can be recovered using the following equation:

$$X_{original}(k) = \frac{X_{difference}(k)}{1 - \exp\left(-j\frac{2\pi k}{N}\right)} \tag{9}$$

The derivation of the Samulon difference FFT algorithm is given in Appendix C.

3.3.2 Simplifications in the improved FFT algorithm

We need to get the transfer function of the DUT by deconvolving the response of the system from the excitation. The denominator in the equation (9) is present in the frequency domain parameters of the excitation as well as in those of the response.

Because of that, as we deconvolve the system response from the excitation, the denominators for those functions in (9) cancel out.

Furthermore, there is no need to deconvolve the response of the system from the excitation. Since the DUT as well as calibration standards frequency domain parameters are the product of the corresponding transfer function and the excitation functions, the frequency domain excitation function cancels out in the process of calibration (see Appendix D). Therefore we can directly substitute the difference waveform spectra for the transfer functions of the DUT and calibration standards.

3.3.3 Choices for the acquisition window shape

When we take the FFT of the data acquired using a finite acquisition window, we effectively impose the rectangular window on the data. This is equivalent to the convolution of the data spectrum and the rectangular window spectrum in frequency domain. Convolution of the window function and the data smoothes the spectrum of the data provided that the spectrum of the window is narrow compared to the spectrum of the data (i.e. the length of the window is sufficiently large). Even if the window spectrum is narrow compared to the data spectrum, the convolution of the data spectrum with the sidelobes of the window spectrum will results in the energy leakage in the frequencies where the actual signal may not have had any energy. To reduce this leakage, a window without sidelobes in frequency domain can be used,

such as Blackman, Hanning or Hamming. Such window would have a smooth time domain cutoff. It would eliminate sidelobe leakage, but increase the smoothing and broadening of the data spectrum [39]. Examples of such windows are shown in Appendix E.

The accuracy of the Samulon method (as well as any of the other methods described in [30-38]) is sensitive to the start and end point noise. Using windows with smooth time domain cutoff will allow to take care of the noise effects.

3.3.4 Extracting the value of the data spectrum at zero frequency

The value of the data spectrum at zero frequency (the DC value) is effectively an average value of the data time domain waveform. Therefore, it is often dependent on the length of the acquisition window. The DC value obtained from the data with finite length of the acquisition window may be different for different window lengths and *incorrect.*

Consider, for example, a DC value for an ideal inductor. Theoretically its DC value must be equal to unity. In practice it can be found as the ratio of the average values of the time domain waveforms for the ideal inductor response and measurement system stimulus. Evidently, the DC value will be less than unity if we try to obtain it using the TDR measurements with finite time length of the acquisition window (see Fig. 4).

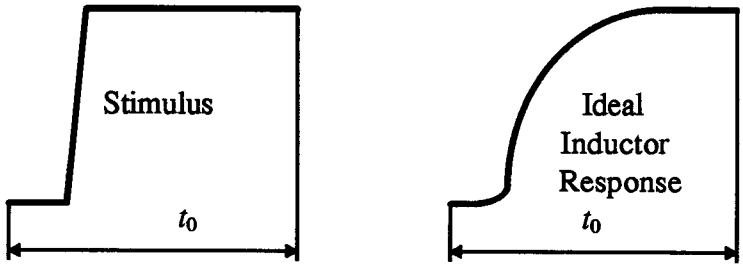

Fig 4. Effect of finite length of the acquisition window on the value of the data spectrum at zero frequency for an ideal inductor example. The zero frequency data spectrum value is dependent on the time length of the window

We can estimate the correct DC value from the time domain start and end point values. We substitute the difference between these values as the DC value for all DUT and calibration standard, and then recover the DC value of the DUT using the frequency domain error correction.

This DC value is very susceptible to the start and end point noise errors. To deal with this problem, we need to use a set of start and end point values rather

Fig 5. Estimating the start and end point values

than a single point values. Our solution was to find a straight line fit for the 5% of the points at the start and the end of the waveforms and then get the start and end point values from this straight line fit.

This approach effectively gets and the average start and end point values. At the same time it is less dependent on the assumption that the DUT transients are settled down by the end of the acquisition window than the direct averaging of the start and end points.

3.3.5 Effective power of the system

The effective power of the system stimulus is that of the step processed using the improved FFT algorithm (Samulon method in our case). The dependence of the power on frequency is described by the equation ([40], see also Appendix F):

$$P = \left(\frac{A}{\pi \cdot f \cdot T} \right)^2 \tag{10}$$

where A is the amplitude of the step excitation, T is the length of the acquisition window, and f is the frequency.

It follows from this equation that the effective power of the system stimulus decreases with frequency and is reverse proportional to the time length of the acquisition window for the given frequency. Therefore, the shorter the acquisition

window, the higher the effective power of the stimulus and the dynamic range of the system for the given frequency.

The requirement for the shorted window for higher dynamic range is conflicting with the requirement of a longer acquisition window lengths, which is necessary to get all the DUT transients in the acquisition window. It is up to user to find the appropriate compromise for the best results.

3.3.6 Frequency domain interpolation

The acquisition window length for the time domain data defines the frequency domain data step as follows:

$$f_{step} = \frac{1}{T} \tag{11}$$

where T is the length of the time domain acquisition window. Sometimes this would give unsatisfactory frequency domain resolution. However, it is possible to interpolate the frequency domain data through the digital interpolation or zero padding [39], see Appendix G. It is important though that all the transients characterizing the DUT settle within the acquisition window. Under this condition, the interpolation gives physically meaningful results.

3.4 Recovering the Enhanced Accuracy Time Domain Waveforms

The frequency domain calibration techniques together with the improved FFT can be used to obtain an EA-TDR/T waveform. To get the EA-TDR/T waveform, the frequency domain parameters of the DUT obtained using FFT and OSL(T) calibration procedure, are multiplied with an ideal excitation and the inverse FFT of the obtained spectrum is taken to get the EA-TDR/T waveforms. The time domain response to the ideal step excitation can be obtained using the following equation:

$$x_{DUT\ ideal\ step}(n) = \sum_{m=0}^{n} \mathrm{IFFT}_m \left\{ \mathrm{FFT}_k \left[x_{ideal\ pulse}(l) \right] \cdot X_{\mathrm{A}}(k) \right\} \tag{12}$$

It is preferable to use an ideal pulse instead of an ideal step excitation, and then integrate the pulse response in time domain to obtain the time domain results corresponding to step excitation. The linear property of the FFT processing (see Appendix H) allows us to do that. This way we can avoid the necessity of improved Inverse FFT (IFFT) algorithms for step-like waveforms.

A Gaussian pulse described by equation (13) has the desired shape in time and frequency domains to allow filtering of the high-frequency noise contribution:

$$x(n) = \mathrm{V} \cdot \exp\left(-\frac{\left(t(n) - t_{middle\ point} \right)^2}{2 \cdot \sigma^2} \right) \tag{13}$$

where V is the step amplitude and σ is an empirical parameter that determines the rise time of the desired step excitation. When defining the value for parameter σ, one need to remember that pulse has high frequency harmonics in both rising and falling slopes.

Because of that, the rise time of the pulse must be half that of the desired ideal step excitation.

Because of the finite rise time of the physical excitation in our measurements, we have information about the DUT only up to the frequencies determined by this excitation rise time and the noise floor of our measurement system. The risetime of the ideal excitation can be chosen to be faster than that of the original excitation. There is a trade off, however, between excessive high-frequency noise and speed of the ideal excitation signal. The noise contribution may results in loss of the resolution required to discern the details of the DUT.

4. ERROR ANALYSIS

4.1 Hardware errors

4.1.1 Vertical (voltage or impedance) scale errors

We can decrease the *noise floor* in the system and correspondingly improve the Signal-to-Noise Ratio (SNR) of the system for the given bandwidth by increasing the number of averages or the number of points in the acquisition window [28]. Moreover, increasing the number of averages or number of points we increase the SNR as follows:

$$SNR(N, N_{avg}) = SNR(N_0, N_{avg\,0}) \cdot \sqrt{\frac{N}{N_0}} \cdot \sqrt{\frac{N_{avg}}{N_{avg\,0}}} \tag{14}$$

where N_o, $N_{avg\,0}$ are the initial and N, N_{avg} are the final number of points and averages in the acquisition settings.

In order to further improve SNR of the system, we can keep the acquisition window short, increasing the effective power of the system stimulus signal.

The *quantization error* is defined in case of rounding as half of the Least Significant Bit (LSB) in the analog-to-digital (A/D) converter. Assuming that the quantization error is significantly bigger than the noise floor, the SNR in a digital sampling system is determined by the A/D converter resolution, or by the number of

bits in the A/D converter. Each additional bit adds 6 dB to the SNR of the system [29],

$$\Delta \mathrm{SNR} = 6 \cdot \mathrm{b} \tag{15}$$

where b is the number of bits.

If the noise floor and the quantization error levels are comparable, they both contribute to the deteriorating of the SNR. It is preferable, however, to have the noise floor dominate the quantization error. In that case we are able to recover some values of the signal that would otherwise have been buried under the quantization error. It is sometimes even preferable to add artificial noise or *dither* at the input of the A/D converter, and then filter it out after the signal has been digitized [41,42].

4.1.2 Horizontal (time base) scale errors

The effect of the *time jitter* on the averaged time domain data has been shown to be that of a low pass filter [24,25]. The time domain impulse response of this filter is defined by the probability density function (pdf) of the jitter itself, and can be deconvolved from the system response [24].

The *time base nonlinearity* in the modern DSO has been analyzed and correction algorithms have been described in [43,44]. These algorithms allow to measure time intervals with high accuracy.

4.2 Signal Processing Errors

The *aliasing errors* can be eliminated if the Nyquist criterion for our data is met. This criterion requires that

$$\Delta t \leq 1/(2 \cdot f_{BW}) \tag{16}$$

where Δt is the time step in the acquisition settings, and f_{BW} is the bandwidth of the data. For practical consideration we can choose f_{BW} to be the specifications bandwidth of our acquisition system.

The *truncation errors* are eliminated if the DUT transients are settled by the end of the acquisition window and are inevitable if this condition is not met.

4.3 System Dynamic Range and Measurement Repeatability

The dynamic range is a parameter normally characterizing the frequency domain measurements. On the other hand, the EA-TDR/T measurements are made in time domain. However, in order to analyze the precision of the EA-TDR/T measurements it is useful to estimate how accurately we recover the parameters for our DUT from the frequency domain point of view. We can do it by applying FFT to the data and analyzing the data spectrum in frequency domain.

The dynamic range that is of interest to us is the system dynamic range. It is defined as the difference between the reference (or stimulus) power in the measurement system and the noise floor of the system for a given frequency [45].

The effect of the dynamic range on the measurement error is as follows. Both noise and signal are vectors in frequency domain, since they are characterized by magnitude and phase. Therefore the summation of the noise and signal in frequency domain is vectorial (see Fig. 6). The superposition of a noise vector with the signal vector occurs the same way the superposition of a small and a large signal would (provided the signal is bigger than noise). The magnitude error is maximum when the vectors of signal and noise have the same or opposite direction, and the phase error is maximum when they are orthogonal. For example, to get the magnitude of the reflection coefficient within 1 dB of precision at a given frequency, we need to have the dynamic range of 24.5 dB. Correspondingly, to get a 0.5 dB of precision for the reflection coefficients magnitude measurements, it is necessary to have the dynamic range of about 30.8 dB [46].

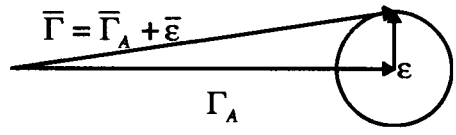

Fig. 6. Vectorial summation of the signal and noise in frequency domain

Practically, the dynamic range can be estimated by measuring the frequency domain parameters of the matched load calibration standard using the OSL calibration

procedure for a one port measurement or by measuring the frequency domain parameters of the through standard using the OSLT procedure for the two port measurements.

5. RESULTS AND DISCUSSION

5.1 Experimental Setup

The measurements were performed with a Tektronix 11801B Digital Storage Oscilloscope (DSO) using a 20 GHz bandwidth SD-24 sampling head. Coaxial cables 2 ns long with 3.5 mm connectors were used. The setup configuration is shown on Fig. 7.

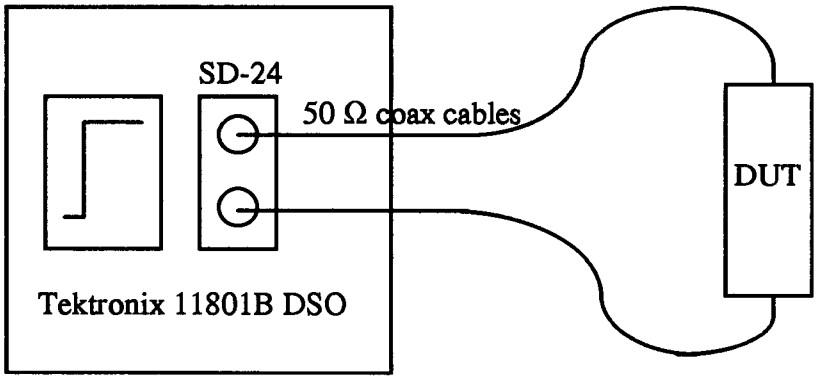

Fig. 7. Experimental setup for the time domain measurements

Experimental time drift correction firmware *TDRCal* for the DSO was employed. Beatty standard, a 25 Ω precision airline terminated in 50 Ω, was used as a

DUT with high reflection coefficient and a 20 dB through pad terminated in a short was used as a DUT with low reflection coefficient. These verification standards can be found in the Hewlett Packard 85053B Verification kit. Hewlett Packard 85052B Calibration kit was used in the OSL(T) frequency domain calibration procedure. The expected frequency domain waveforms are shown in the Appendix I.

Even though the bandwidth of the SD-24 sampling head is 20 GHz, most measurements were taken up to 30 GHz to get a better understanding of the system performance.

5.2 General Considerations

The measurements settings were chosen according to the general analysis in previous sections, to have the shortest acquisition window possible with all the transients characterizing the DUT included in the window. This way we provide maximum effective power in the system (see Section 3.3.5), while minimizing the truncation errors (see Section 4.2). For Beatty and 20 dB through standards the settings for the Tektronix 11801B DSO were as follows:

- time base – 200 ps/division (acquisition window – 2 ns)
- averaging on, 128 averages
- number of points 1024
- hardware smoothing off

Hardware smoothing decreases the noise floor before the signal enters the A/D converter. It may have an undesirable effect on the measurement system resolution, as it is discussed in Section 4.1.1. Turning the hardware smoothing off, together with more heavy averaging after the signal went through the A/D converter, potentially allows us to recover more information about the signal.

As it is discussed in Section 3.3.3, we may benefit by applying window with

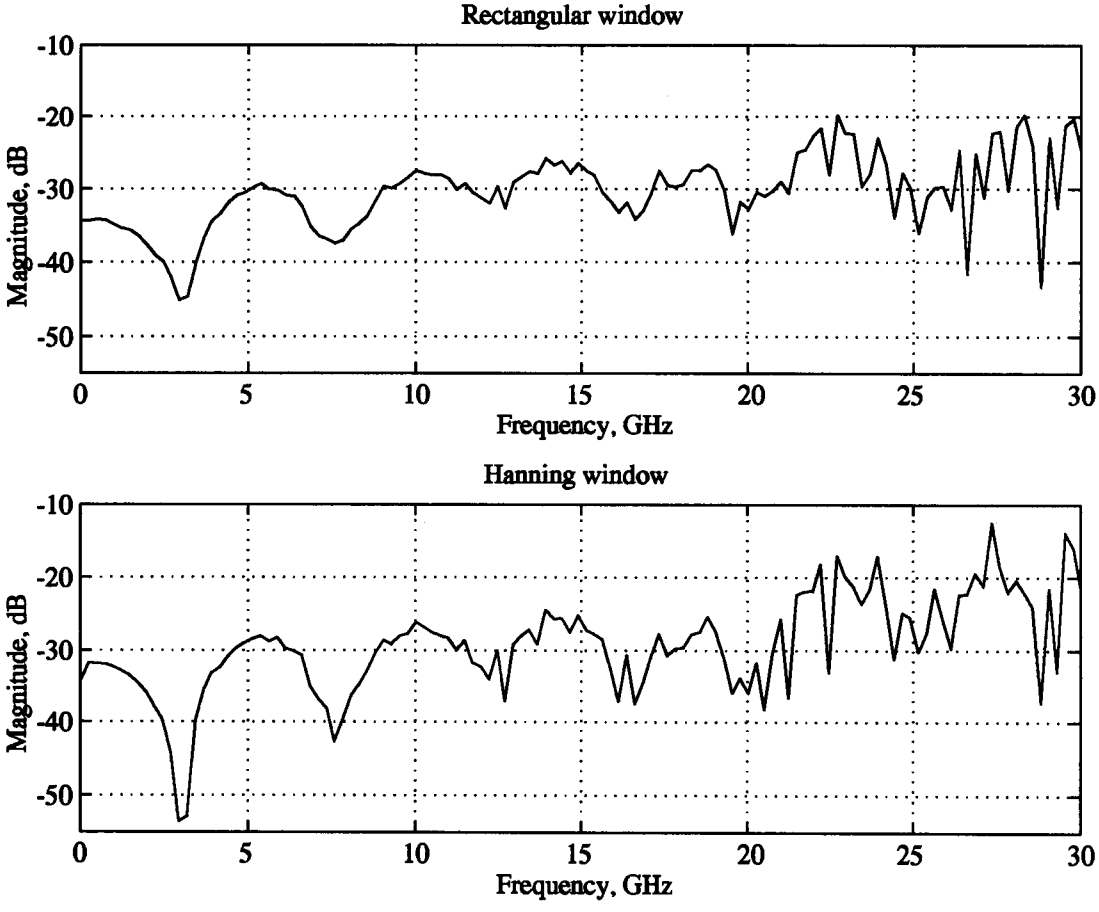

Fig. 8. Spectra of the reflection coefficient of a 20 dB through pad terminated in a short obtained by rectangular and Hanning windows applied to the data

low sidelobes in frequency domain to the acquired data. We experimented with different windows and some of the results are shown on Fig. 8.

From this results one can not make a clear decision about whether low frequency domain sidelobes window like Hanning is better than the rectangular. On the other hand, the rectangular window is simpler to deal with when transforming the data between time and frequency domains.

It is necessary, however, to eliminate the dependence of the spectrum on the data start and end point noise. A window with low time domain cutoff would take care of that by forcing the start and end points to zero.

The reasonable compromise is to apply the rectangular window to most of the data, and apply a low time domain cutoff window to the start and end points of the data. This is the path we chose to follow, applying the Hanning window to the 5% of the points on both ends (left part of the window at the start and right side of the window at the end, see Appendix E).

5.3 Error Analysis for the Measurement System Under Consideration

5.3.1 Vertical (voltage or impedance) scale errors

Quantization error

As it has been discussed in Section 4.1.1, it is undesirable to have the quantization error larger than the noise floor of the system. For 50 mV per division vertical scale settings in the Tektronix 11801B DSO, we will get the LSB of about 2 mV, or quantization error of 1 mV (see Appendix J). For 200 mV per division we will have 4 mV quantization error.

When the hardware smoothing in the Tektronix 11801B DSO is on, the signal enters the A/D converter in the DSO with its noise floor significantly reduced. Therefore for certain vertical scale settings in the DSO we may encounter the undesirable situation when the noise floor is lower than the quantization error, as it is shown on Fig. 9.

If this happens, we may actually lose rather than gain from the hardware smoothing in the Tektronix 1180B DSO. As noise floor decreases compared to the quantization error, we lose more resolution, that would otherwise have been achieved by the averaging after A/D conversion (see Fig. 9).

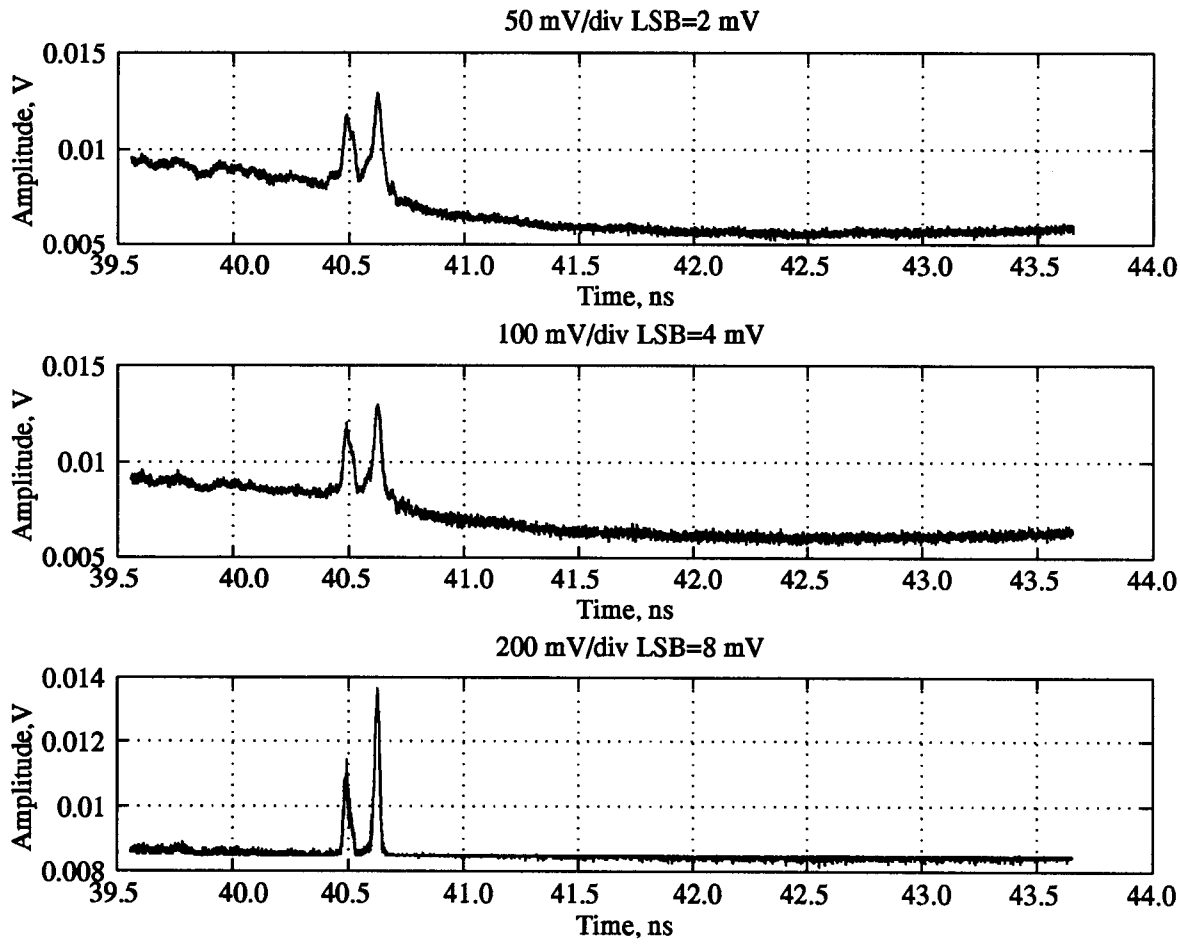

Fig. 9. Quantization error vs. noise floor. If the quantization error is bigger than the noise floor, we may not be able to recover some data values

Sampling head amplitude change with DC loading

The amplitude of the SD-24 step change about 2 mV as DC load changes from short to 50 Ω and from 50 Ω to open. This effect is due to the bias network of the step generators.

The effect of the amplitude change has been investigated by simulating the circuit with different amplitudes of the excitation step depending on the termination. TekSPICE simulation software was used. The simulations were performed for Beatty standard. The results of the simulations are shown on Fig. 10.

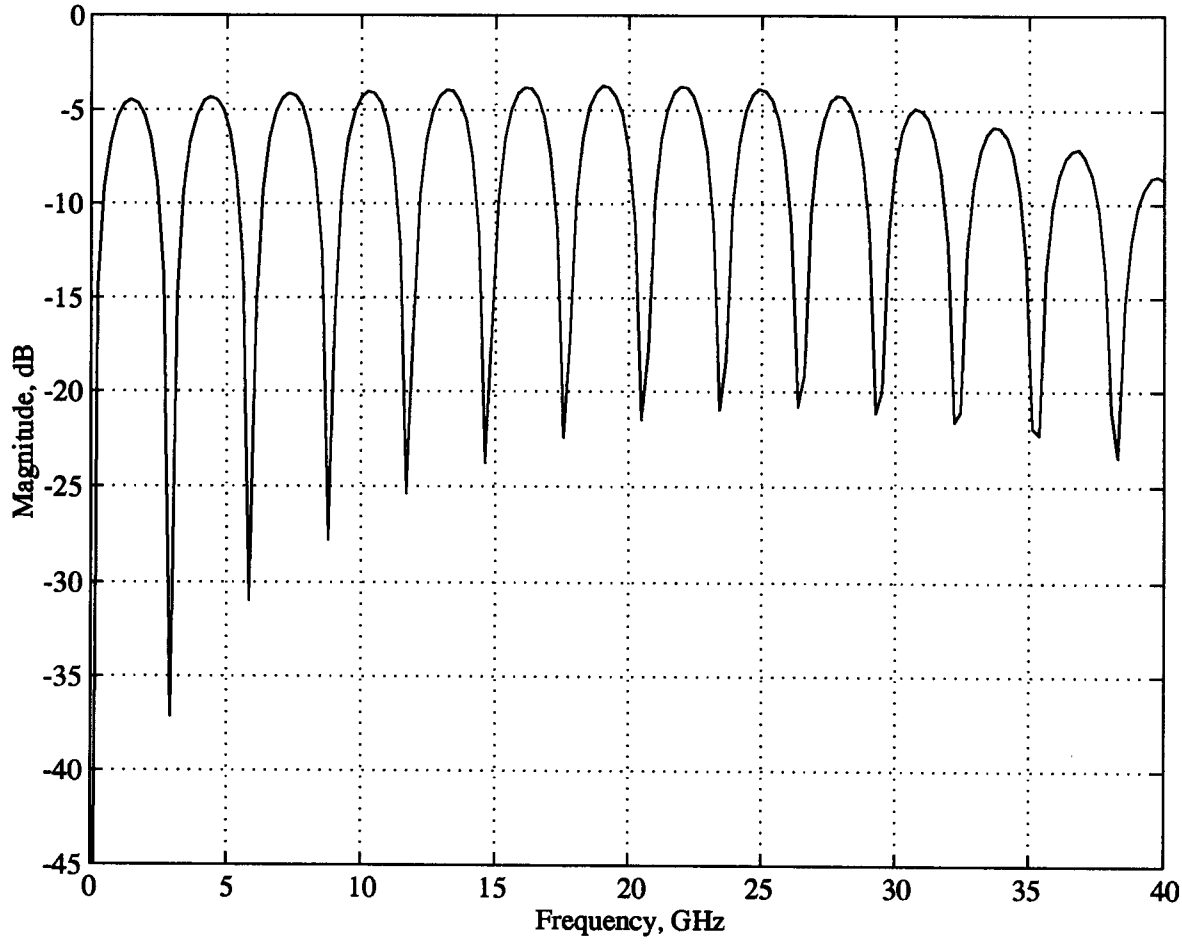

Fig. 10. Simulation of the effect of different step amplitudes for different terminations on the time domain measurement results

The simulation do not show any significant effect on the frequency domain data below 30 GHz. However, there is a roll-off of the data values at frequencies above 30 GHz. Therefore we can conclude that the effect of step amplitude change is small within the frequency range of interest, but it may be potentially dangerous.

5.3.2 Horizontal (time base) scale errors

Jitter

As it is discussed in Section 4.1.2, the effect of time jitter with averaging is that of a low pass filter with the impulse response of this filter being the probability density function of the time axis jitter. For Tektronix 11801B DSO the rise time of this filter impulse response is 2-3 ps [43], which corresponds to a cutoff frequency of more than 100 GHz. This is significantly above the highest frequency of interest (20 GHz) and should not affect our measurements.

Drift

The long term time drift is caused by thermal effects due to changing the operational mode of the DSO and ambient temperature changes.

To understand how much error time drift can cause, the simulations using TekSPICE have been performed. The data waveforms have been shifted by a few picoseconds relatively to the calibration waveforms, and the frequency domain error correction was performed.

As it can be seen from Fig. 11, even a drift of a 2 ps can cause a 1 dB error at 20 GHz, and 4 ps drift — 2 dB at the same frequency. In real life the time drift is random, which may lead to even bigger error values than those obtained from the

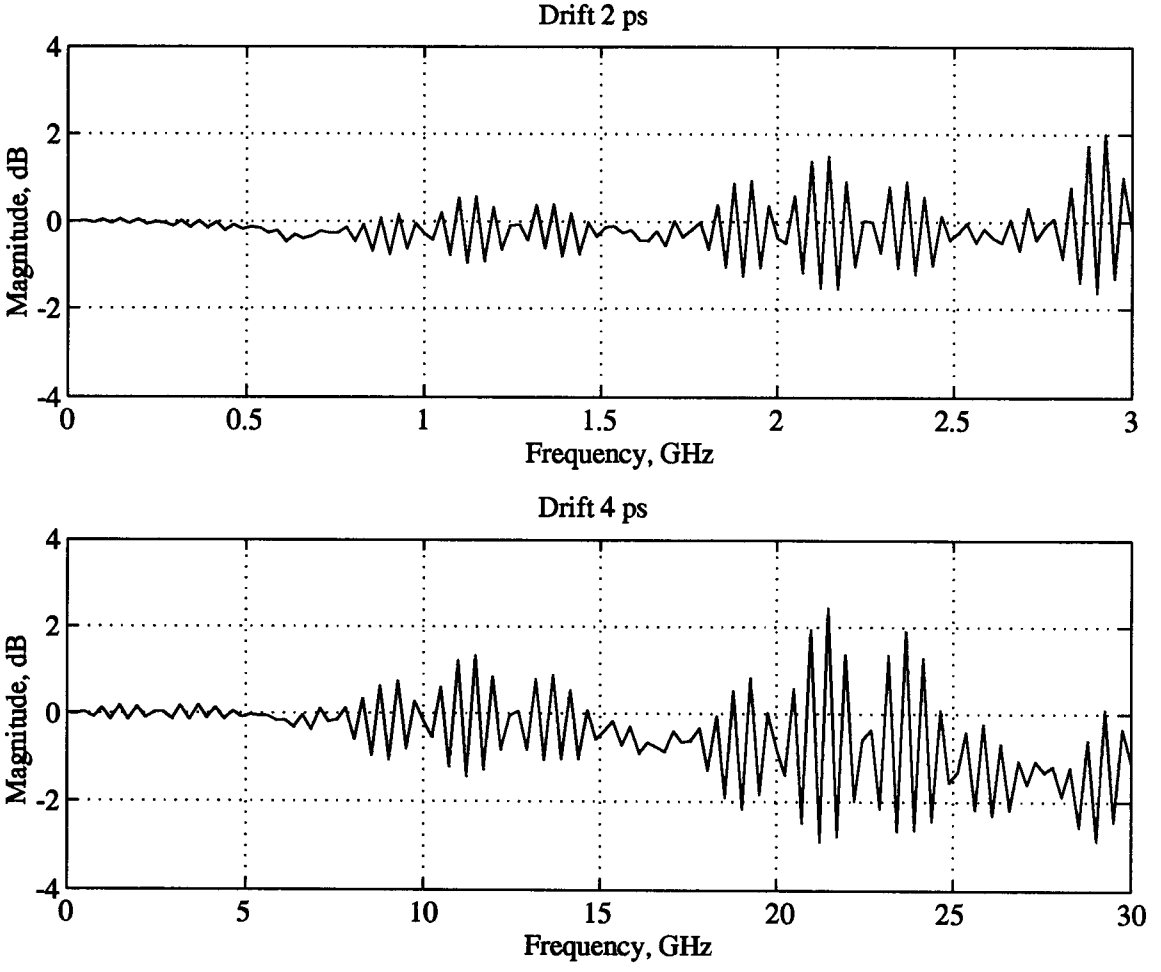

Fig. 11. Time drift simulations. The data waveform (corresponding to a short termination as DUT) is shifted by 2 and 4 ps relatively to the calibration waveforms. In real life the time drift is random, which may lead to even bigger error values than those obtained from the simulations

simulations.

To correct for the drift in the Tektronix 11801B DSO, the software *TDRCal* has been developed and added in the firmware to the Tektronix 11801B DSO. This software allows us to restrain the time drift within an arbitrary small time value. It finds the incident edge of the excitation pulse, and since this edge is independent of the reflection of the DUT, it uses it as a reference for all the consequent waveforms. We used the correction within 0.5 ps, which allows us to keep the amplitude error with 0.25 dB at 20 GHz.

To get an ultra high precision for timing measurements, Tektronix 11801B DSO employs a time base nonlinearity correction algorithm [43], which decreases the peak-to-peak error for the timing measurements down to 1.5 ps at the 30 ns interval measurements. However, this algorithm conflicts with *TDRCal* and needs to be turned off during the measurements. The precision of the timing measurements suffers insignificantly, while the fine drift correction algorithm allows us to get high accuracy EA-TDR/T measurements.

5.3.3 Dynamic range

The following measurements have been taken to illustrate the dependence of the dynamic range on the number of averages.

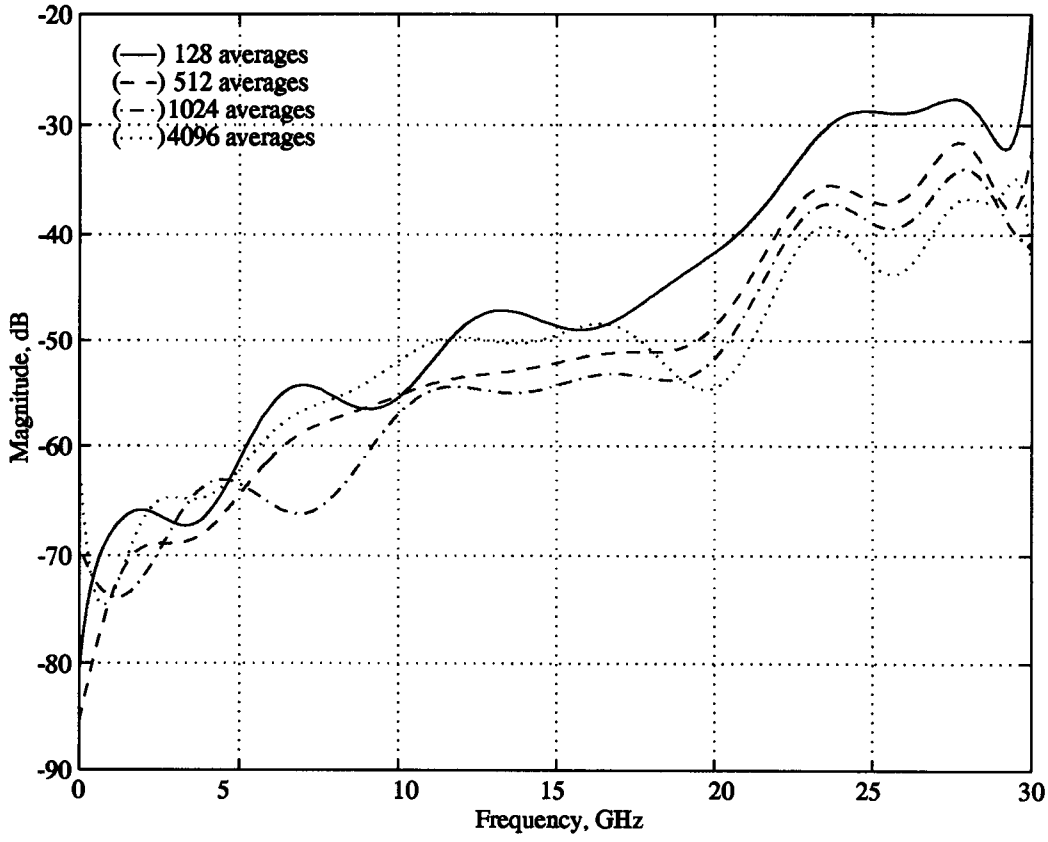

Fig. 12. Dynamic range of the system for different number of averages. Averaging is performed in time domain. As the number of averages increases, system encounters the quantization error. The appearing deterioration of the dynamic range as the number of averages goes to 4096 should be attributed to short term temperature-related drift

As one can see, as we go from 512 to 1024 and 4096 averages, there is no actual improvement in dynamic range at the regions where it has values below -60 dB. Obviously, we encounter the quantization error in these regions. The apparent deterioration of the dynamic range as we go to 4096 averages should be attributed to the temperature-related drift.

If we used hardware smoothing, quantization error would begin to show up more quickly, as we discussed in Section 4.1.1.

The effect of the dynamic range on the accuracy of the measurements is illustrated on Fig. 13 . As the number of averages increases, our accuracy improves as the dynamic range improves.

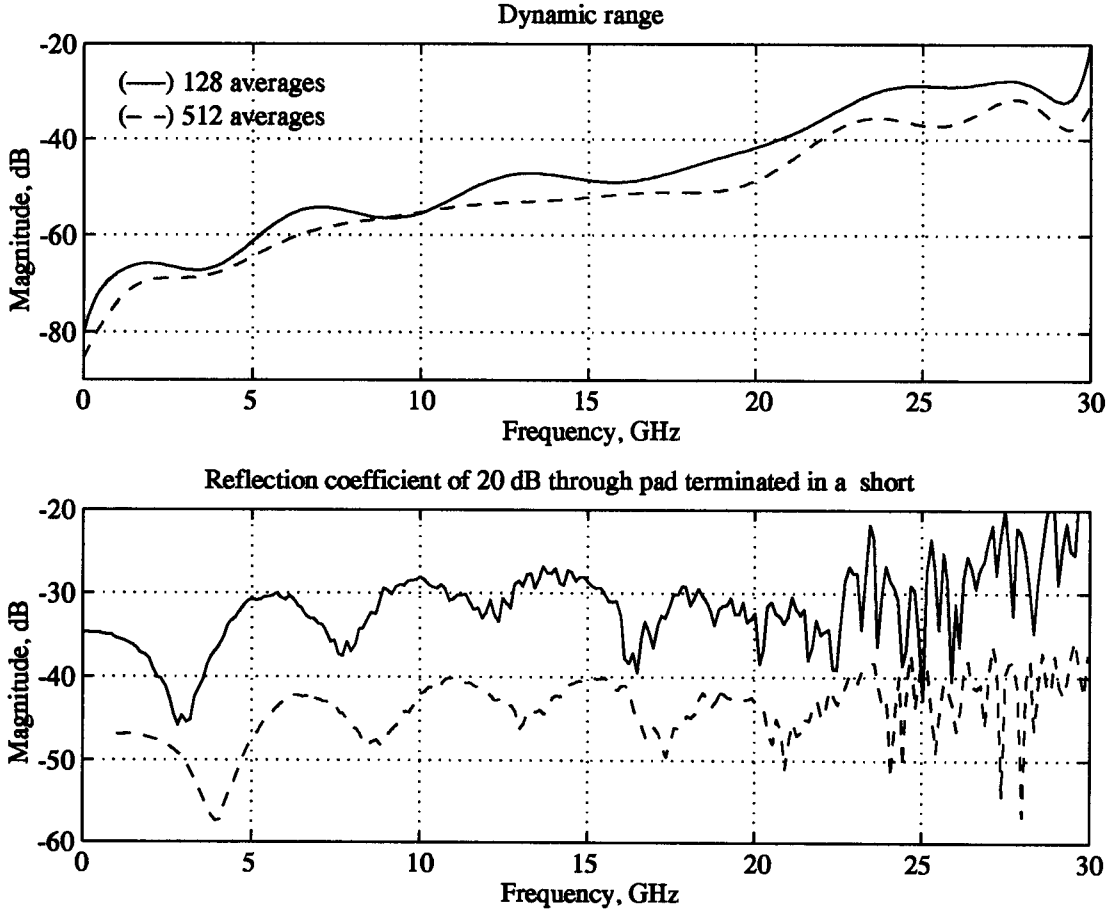

Fig. 13. Effect of the dynamic range on the accuracy of the measurements. As the number of averages increases, our dynamic range increases, and the accuracy of our measurements improves. Waveforms are offset for display purposes

5.4 One-Port Measurements

5.4.1 Effective power of the system

The ideal step equivalent power and the power of the step launched by the SD-24 sampling head is shown on the Fig. 14. The system settings are 4096 points and

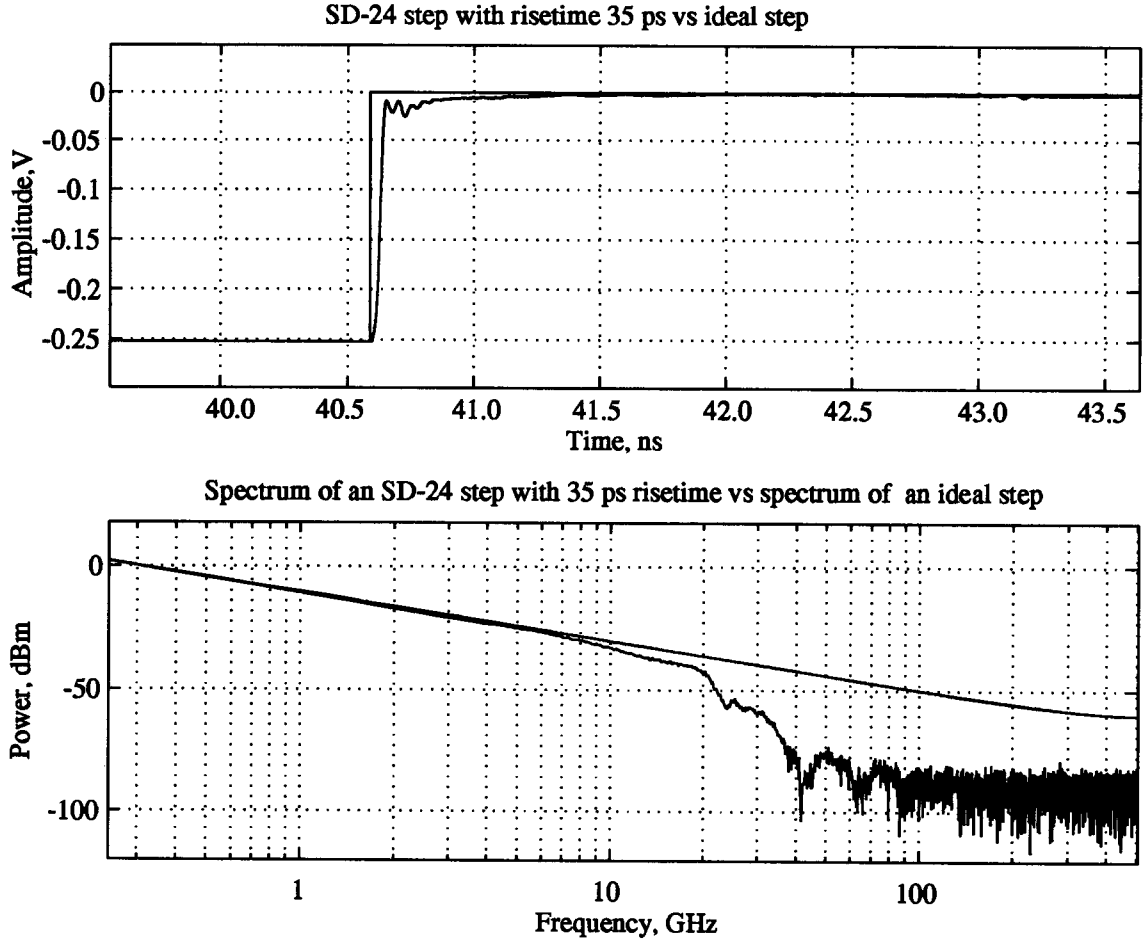

Fig. 14. Power spectrum of a step excitation

500 ps/division.

The cutoff frequency for an SD-24 step is 20 GHz. There is some power in the stimulus up until about 40 GHz, when it hits the noise floor. This allows us to take valid measurements above 20 GHz, provided our dynamic range is sufficient for the given DUT.

5.4.2 Repeatability of measurements

There is significant amount of error due to nonrepeatability of the measurement. It is hard to assess how much error is introduced by this problem, since a big number of measurements is necessary to obtain reliable statistics.

To estimate the repeatability of the measurements, several measurements over a period of time have been performed for the reflection coefficient of 20 dB through pad terminated in a short using Tektronix 11801B DSO and Hewlett Packard 8510B network analyzer. The network analyzer measurement is given for comparison. The results of these measurements are shown on Fig. 15.

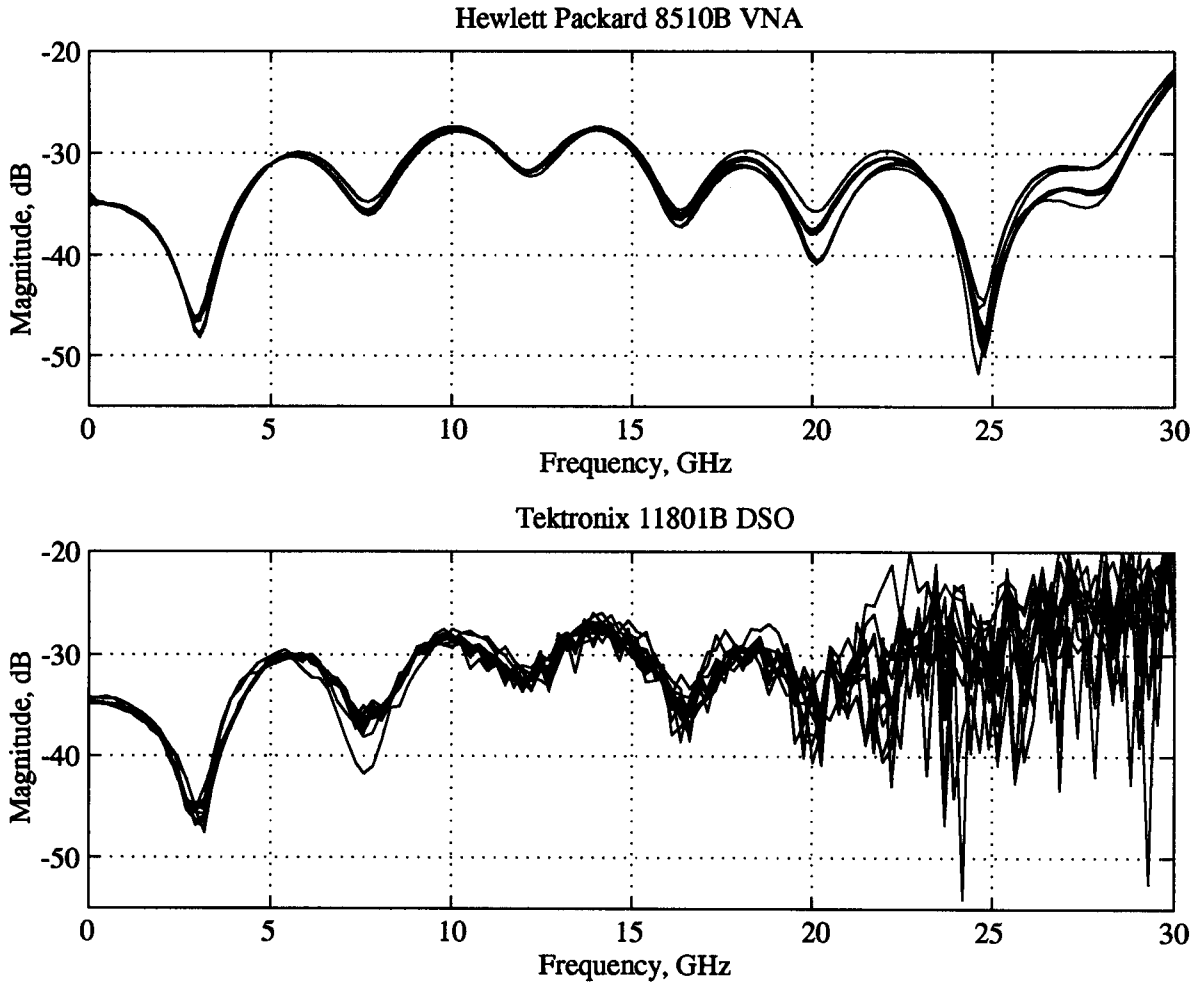

Fig. 15. Repeatability of frequency domain results for Tektronix 11801 B digital storage oscilloscope and Hewlett Packard 8510 B vector network analyzer. Data are shown for the reflection coefficient of 20 dB through pad terminated in a short. 14 measurements have been performed using Tektronix 11801 B DSO and 12 measurements using Hewlett Packard 8510 B VNA over a significant period of time. The poor repeatability for the both systems can be attributed to breaking and restoring the connection at the DUT reference plane and flexing of the cables

Our error analysis shows that there are no errors that would be able to cause such significant nonrepeatability. Therefore the nonrepeatability for both systems can be attributed to the mechanical errors of breaking and restoring the connection at the DUT reference plane, as well as the flexing of the cables in the measurement system.

5.4.3 EA-TDR and Z-profile results and analysis

After analyzing the frequency domain results, we can proceed to obtaining the EA-TDR waveform, following the algorithm in Section 3.1.

Parameter σ depends on the defined equivalent step excitation risetime as

$$\sigma = \frac{t_{rise}}{2.564} \tag{17}$$

In that case a step waveform obtained by integration (summation in discrete case) of a pulse waveform will have a risetime of t_{rise}, with the precision of ± 1 ps.

The effect of different rise times defined for our excitation is that of a lowpass filter in frequency domain, for which different rise times give different cutoff frequency. Therefore the risetime of the excitation defines a tradeoff between how much noise is present in the TDR waveform and how well the shape of the waveform is preserved.

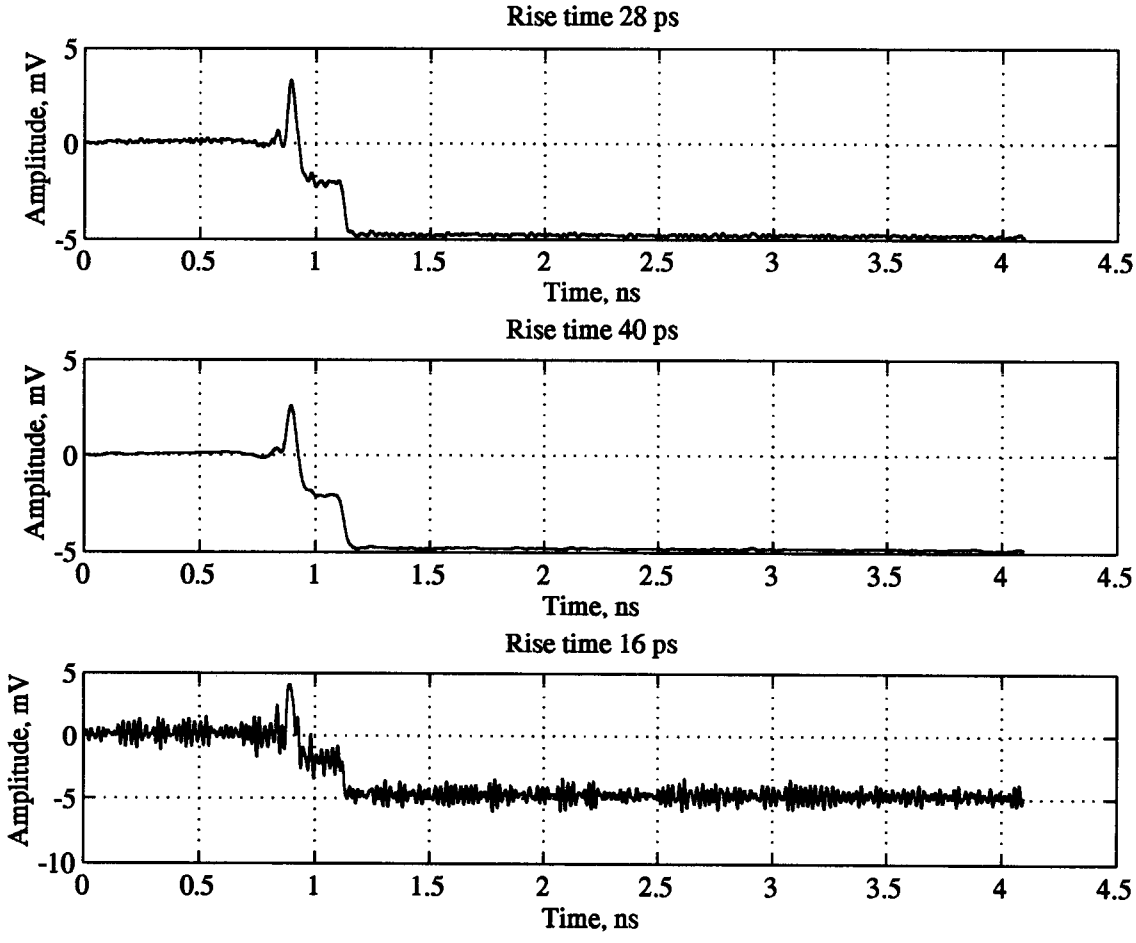

Fig. 16. The time domain waveforms of a reflection coefficient of a 20 dB through pad terminated in a short shown for different excitation rise times

Fig. 16 illustrates this statement. Clearly, optimal equivalent step excitation risetime is about 28 ps. A rise time of 40 ps gives TDR waveform of the 20 through pad terminated in a short with much lower noise floor, but some deterministic

information is lost as well. For the rise time of 16 ps we get unacceptable noise floor, which does not allow clear observation of the deterministic features of the waveform.

Fig. 17 illustrates the error corrected TDR waveform of 25 Ω precision airline (Beatty standard) as compared to the original one. As it was expected, the EA-TDR waveform gives much more accurate TDR waveform for the Beatty standard.

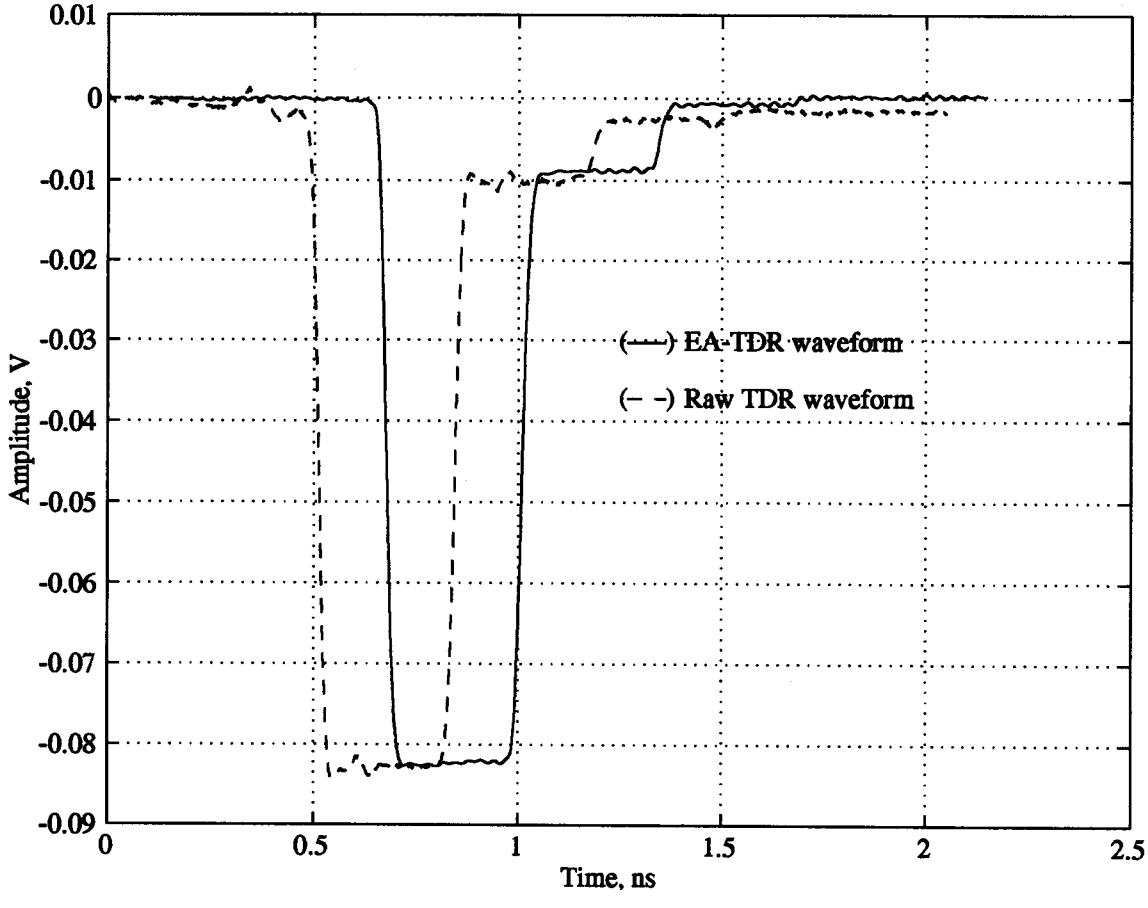

Fig. 17. EA-TDR Beatty standard waveform vs. the raw TDR waveform. Waveforms are offset for display purposes

Now we can apply the Z-profile algorithm to the EA-TDR waveform to obtain the actual impedance profile of the DUT. The slope of the impedance profile waveform is due to the losses in the airline [48].

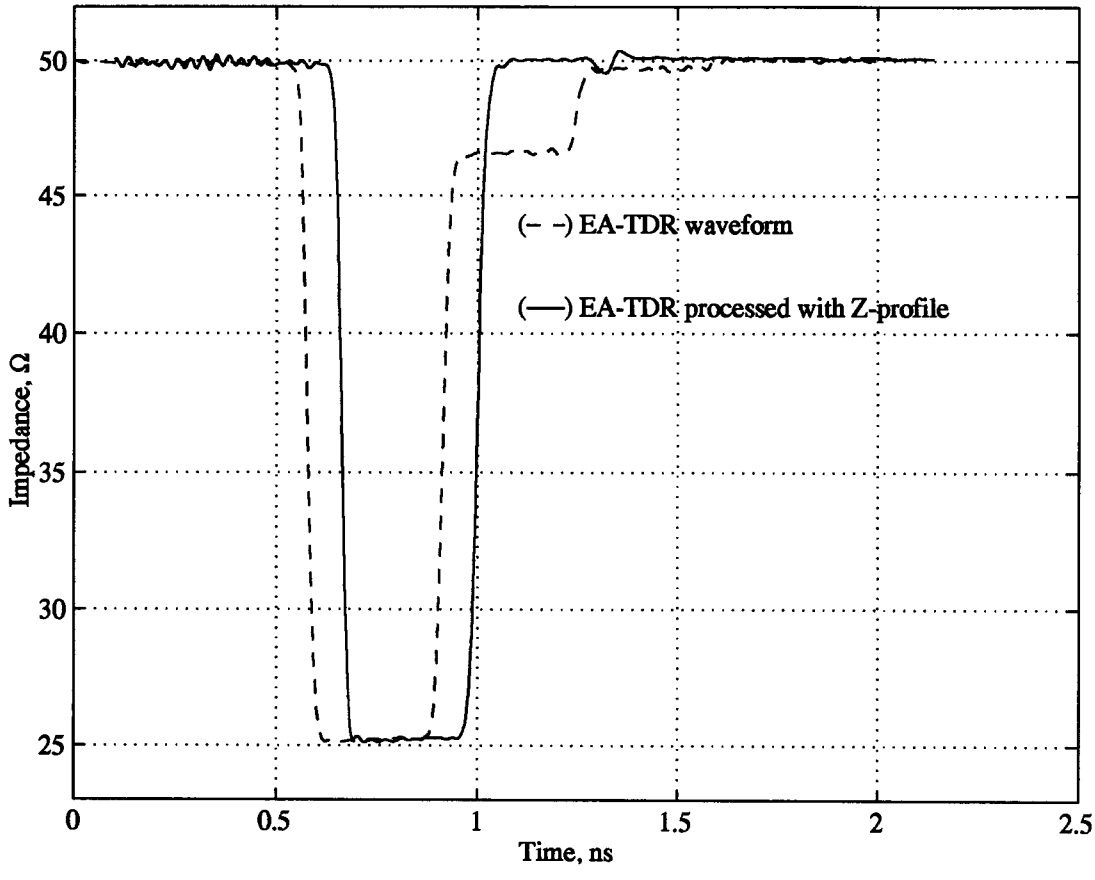

Fig. 18. The Z-profile algorithm applied to the EA-TDR waveform. The actual impedance profile is recovered. The y-axis is in ohms for convenient impedance readout. Waveforms are offset for display purposes

5.5 Two-Port Measurements

The same approach is applied to the two port measurements. As a results, we can get an Enhanced Accuracy TDT measurement (EA-TDT).

The EA-TDT measurement for the Beatty standard is shown on Fig. 19

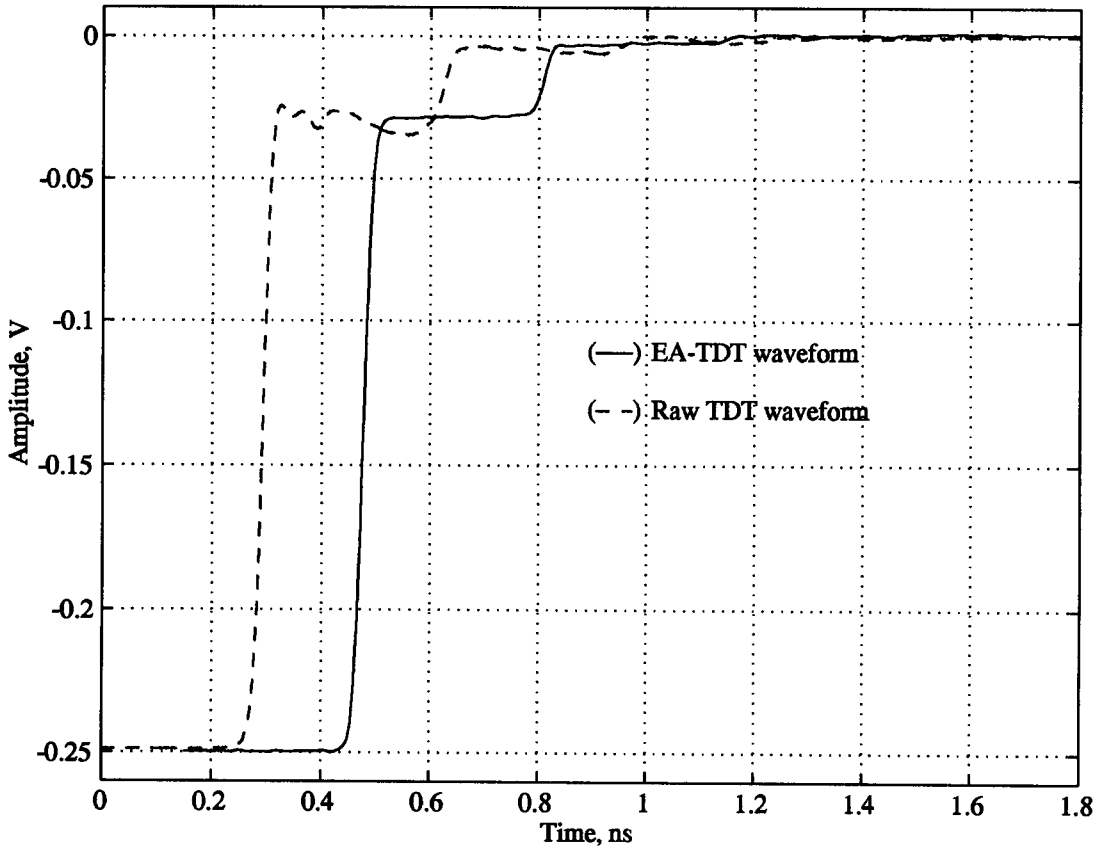

Fig. 19. EA-TDT measurements for the Beatty standard. Waveforms are offset for display purposes

5.6 Frequency Domain Measurement Results

The following figures illustrate TDNA measurements obtained using Tektronix 11801B DSO and the FDNA ones obtained using Hewlett Packard 8510B Vector Network Analyzer (VNA) for Beatty standard and 20 dB through pad terminated in a

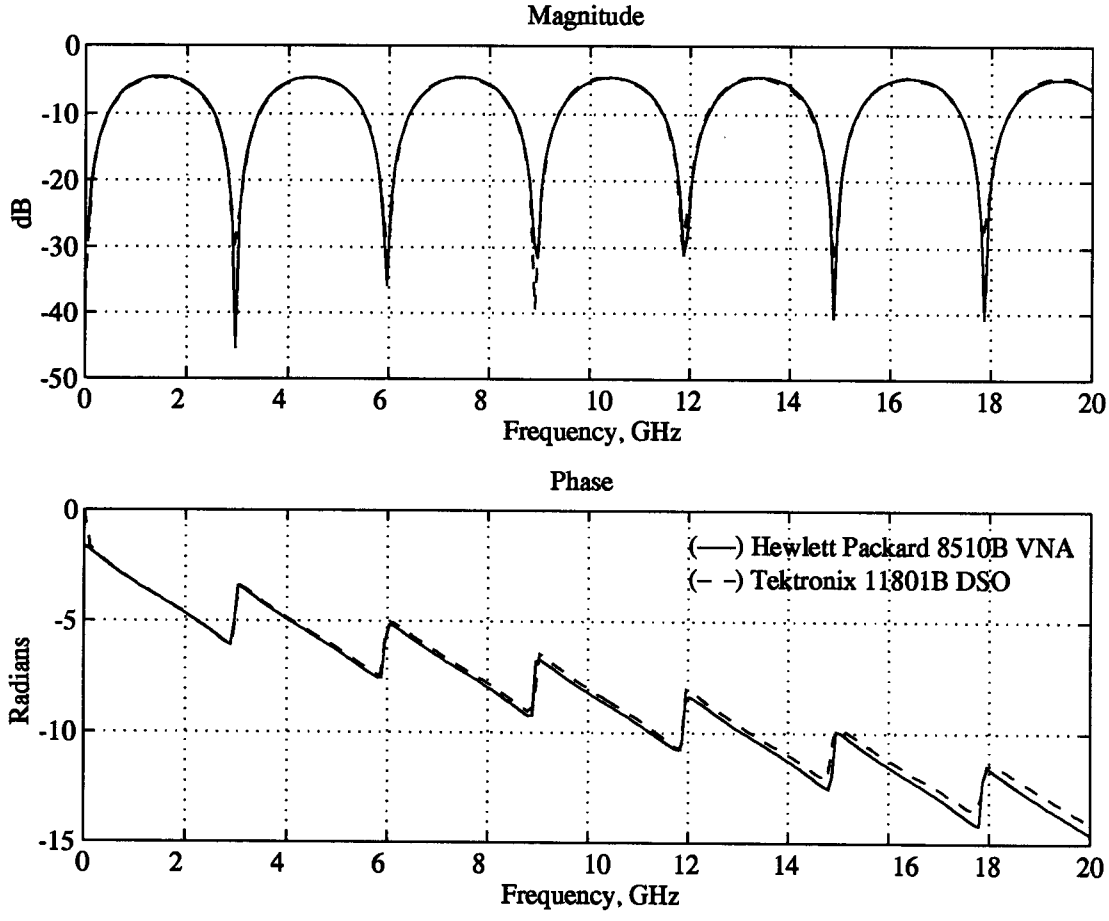

Fig. 20. Beatty standard TDNA measurement obtained using Tektronix 11801B digital storage oscilloscope and FDNA ones obtained using Hewlett Packard 8510B vector network analyzer

short. The difference between the two measurements lies well within the error specifications for the VNA system.

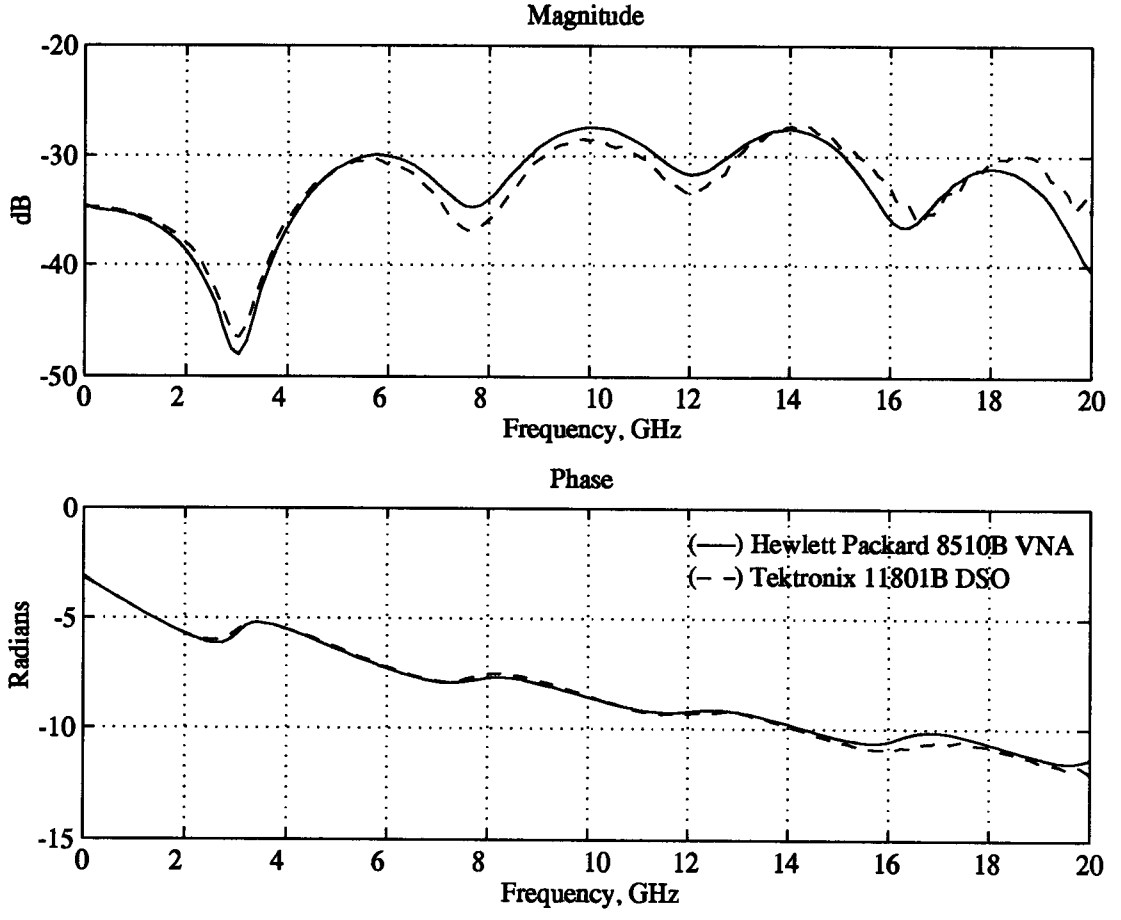

Fig. 21. 20 dB through pad terminated in a short TDNA measurement obtained using Tektronix 11801B digital storage oscilloscope and FDNA ones obtained using Hewlett Packard 8510B vector network analyzer

6. CONCLUSION AND SUGGESTIONS FOR FUTURE WORK

In this report, enhanced accuracy time domain reflection/transmission measurement technique has been presented. The technique allows for the accurate characterization of unknown devices under test in terms of an impedance profile as a function of time. The errors in the system and their contribution to the overall measurement error have been analyzed. The repeatability of the system is limited by the mechanical errors due to restoring and breaking the connection between the DUT and the calibration standards, as well as the flexing of the cables.

Further improvement of the system is in the area of better frequency domain error correction techniques, as well as the development of the hardware dedicated to the frequency domain error correction. This means employing thru-reflect-line and other multiline frequency domain calibration techniques [20], and using pulse-like stimulus signals, which have larger high-frequency components and will allow for higher dynamic range in a time domain measurement system. Time domain calibration technique reported in [49] is an attractive idea, but it requires some a priori knowledge about the measurement system or additional high-bandwidth signal source.

Analysis of the deconvolution techniques in the presence of noise is warranted. The issue here is that a frequency domain deconvolution requires filtering in one form or another to decrease the noise effects. The results obtained using these deconvolution and filtering techniques are only the best estimates of the true

ones [50]. Choosing the optimum parameters for the filters employed in the frequency domain deconvolution allows one to get the best estimate with the least amount of noise. Causal nature of the real signals needs to be taken into account as well. If a causal filter is employed, higher accuracy estimate for the DUT parameters can be obtained [51].

Interconnect losses need to be characterized by formulating accurate procedures to extract the loss parameters for the EA-TDR/T. One of the challenges here is to distinguish between the variations in the DUT impedance and the impedance profile slope due to the skin effect. Another is the dielectric loss characterization. Reliable, accurate TDR/T or frequency domain techniques for measurements of frequency depended losses associated with interconnects continues to be a challenging problem.

BIBLIOGRAPHY

[1] B.D. Morrison, J.J. Rosenberg, D. A. Gracious, S.F. Margo, "Design Considerations for High-Frequency Digital Systems," - *Electronic Materials Handbook*, Vol. 1, Packaging, 1990

[2] S.B. Goldberg, M.B. Steer, P. D. Franzon, J.S. Kasten, "Experimental Electrical Characterization of Interconnects and Discontinuities in High-speed Digital Systems," - *IEEE Transactions on Components and Manufacturing Technology*, Vol. 14, No. 4, December 1991, pp. 761-765

[3] G.-W. Pan, J.A. Prentice, S.K. Zahn, A.J. Staniszewski, W.L. Walters, B.K. Gilbert, "The Simulation of High-Speed, High-Density Digital Interconnects in single Chip Packages and Multichip Modules," - *IEEE Transactions on Components and Manufacturing Technology*, Vol. 15, No. 4, August 1992, pp. 465-477

[4] J.-M. Jong, L.A. Hayden, V.K. Tripathi, "Time Domain Characterization of Coupled Interconnects and Discontinuities," - *IEEE Microwave Theory and Techniques Symposium Digest*, Vol. 2, May 23-27, 1994, San Diego, CA, pp. 1129-1132

[5] J.-M. Jong, B. Janko, V.K. Tripathi, "Equivalent Circuit Modeling of Interconnects from Time-Domain Measurements," - *IEEE Transactions on Components and Manufacturing Technology*, Vol. 16, No. 1, February 1993, pp. 119-126

[6] "TDR Tools in Modeling Interconnects and Packages," - *Tektronix Application Note*, 85W-8882-0, 1993

[7] F. Grandjean, G. Angénieux, B. Flechét, "Extraction of Equivalent Circuit of Hybrid Microstrip Resistor by Harmonic Measurements," - *Proceeding of International Symposium on Hybrid Microelectronics*, October 19-21, 1992, San Francisco

[8] D.F. Williams, R.B. Marks, Transmission Line Capacitance Measurement, - *IEEE Microwave and Guided Wave Letters*, Vol. 1, No. 9, September 1991, pp. 243-245

[9] V.K. Tripathi, J.B. Rettig, "A SPICE Model for Multiple Coupled Microstrip and Other Transmission Lines," - *IEEE Transactions on Microwave Theory and Techniques*, Vol. 33, No. 12, December 1985, pp. 1513-1518

[10] M.D. Tilden, "Measuring Controlled-Impedance Boards with TDR," - *Printed Circuit Fabrication*, Vol.. 14, No. 2, February 1992

[11] S.L. Salvage, B. Parruck, S.R. Riad, "Wide-Band Device Modeling Using Time-Domain Reflectometry," - *IEEE Transactions on Instrumentation and Measurement,* Vol. 32, No. 1, March 1983, pp. 134-136

[12] R.Y. Yu, M. Kanegawa, M. Case, M. Rodwell, J. Franklin, "A 2.3 ps Time-Domain Reflectometer for Millimeter-wave Network Analysis," - *IEEE Microwave and Guided Wave Letters,* Vol. 1, No. 11, Nov. 1991, pp. 334-336

[13] J.M. Jong, V.K. Tripathi, "Time Domain Characterization of Interconnects Discontinuities in High-Speed Circuits," - *IEEE Transactions on Components and Manufacturing Technology*, Vol. 14, No. 4, August 1992, pp. 497-504

[14] "Z-profile Algorithm," - *Tektronix Application Note,* 85W-8882-0, 1993

[15] J. Williams, "Accuracy Enhancement Fundamentals for Vector Network Analyzers," - *Microwave Journal*, March 1989, pp. 99-114

[16] L.A. Hayden, V.K. Tripathi, "Calibration Methods for Time Domain Network Analysis," - *IEEE Transactions on Microwave Theory and Techniques,* Vol. 41, No. 3, March 1993, pp. 415-421

[17] T. Dhaene, L. Martens, D. De Zutter, "Calibration and Normalization of Time Domain Network Analyzer Measurements," - *IEEE Transactions on Microwave Theory and Techniques*, Vol. 42, No. 4, April 1994, pp. 580-589

[18] W. Su, S.M. Riad, "Calibration of Time Domain Network Analyzers," - *IEEE Transactions on Instrumentation and Measurement*, Vol. 42, April 1993, pp. 157-161

[19] H.-J. Eul, B. Schiek, "A Generalized Theory and New Calibration Procedure for Network Analyzer Self-Calibration," - *IEEE Transactions on Microwave Theory and Techniques*, Vol. 39, No. 4, April 1991

[20] R.B. Marks, "A Multiline Method of Network Analyzer Calibration," - *IEEE Transactions on Microwave Theory and Techniques*, Vol. 39, No. 7, July 1991

[21] L.A. Hayden, V.K. Tripathi, "Thru-Match Short Calibration for Time Domain Network Analyzers," - *IEEE Transactions on Microwave Theory and Techniques Symposium,* Albuquerque, New Mexico, June 1992, pp. 1447-1450

[22] H.M. Cronson, P. G. Mitchell, "Time-Domain Measurements of Microwave Components," - *IEEE Transactions on Instrumentation and Measurement,* Vol. 22, No. 4, December 1973, pp. 320-325

[23] J.R. Andrews, "Automatic Network, Measurements in the Time Domain," - *Proceedings of the IEEE,* Vol. 66, No. 4, April 1978, pp. 414-423

[24] W. L. Gans, "The measurement and Deconvolution of Time Jitter in Equivalent-Time Waveform Samplers," - *IEEE Transactions on Instrumentation and Measurement*, Vol. 32, No. 1, March 1983, pp. 126-133

[25] W.L. Gans, "Calibration and Error Analysis of a Picosecond Pulse Waveform Measurement System at NBS," - *Proceedings of the IEEE,* Vol. 74, No. 1, January 1986, pp. 86-90

[26] W.R. Scott, G.S. Smith, "Error Correction for an Automated Time-Domain Network Analyzer, *IEEE Transactions on Instrumentation and Measurement*, Vol. 35, No. 3, September 1986, pp. 300-303

[27] P. Ferrari, G. Angénieux, B. Fléchet, F. Granjean, J. Chilo, "Characterization of thick film microwave components Using Time Domain Network Analysis," - *Proceedings of the 2nd International Conference on Electromagnetics in Aerospace Applications,* September 17-20, 1991, Politecnico Di Torino, Italy

[28] S. Diamond, S. Pepper, "Decode Dynamic Range in Time/Frequency-Domain Analyzers," - *Microwaves & RF*, September 1993, pp. 102-110

[29] A.V. Oppenheim, R.W. Schafer, *Discrete-Time Signal Processing*, - Prentice Hall, New Jersey, 1989

[30] H.A. Samulon, "Spectrum Analysis of Transient Response Curves," - *Proceedings of IRE*, Vol. 39, 1951, pp. 175-186

[31] A.M. Nicolson, "Forming the Fast Fourier Transform of a Step Response in Time Domain Metrology," - *Electronic Letters*, Vol. 9, July 1973, pp. 317-318

[32] W.L. Gans, N.S. Nahman, "Continuous and Discrete Fourier Transform of Step-Like Waveforms," - *IEEE Transactions on Instrumentation and Measurement*, Vol. 31, June 1982, pp. 97-101

[33] J. Waldmeyer, "Fast Fourier Transform of Step-Like Functions: The Synthesis of Apparently Three Different Methods," - *IEEE Transactions on Instrumentation and Measurement*, Vol. 29, March 1980, pp. 36-39

[34] A. M. Shaarawi, S.M. Riad, "Computing the Complete FFT of a Step-Like Waveform," - *IEEE Transactions on Instrumentation and Measurement*, Vol. 35, No. 1, March 1986, pp. 91-92

[35] T. M. Souders, D. R. Flach, "Accurate Frequency Response Determinations from Discrete Step Response Data," - *IEEE Transactions on Instrumentation and Measurement*, Vol. 36, No. 2, June 1987, pp. 433-439

[36] A. Bennia, N. S. Nahman, "Deconvolution of Causal Pulse and Transient Data," - *IEEE Transactions on Instrumentation and Measurement*, Vol. 39, No. 6, December 1990, pp. 933-939

[37] G. D. Cormack, D. A. Blair, J.N. McMullin, "Enhanced Spectral Resolution FFT for Step-Like Signals," - *IEEE Transactions on Instrumentation and Measurement*, Vol. 40, No. 1, February 1991, pp. 34-36

[38] N. G. Paulter, Jr, R. B. Stafford, "Reducing the Effects of Record Truncation Discontinuities in Waveform Reconstruction," - *IEEE Transactions on Instrumentation and Measurement*, Vol. 42, No. 3, June 1993, pp. 695-700

[39] J.G. Proakis et al, *Advanced Digital Signal Processing*, - Macmillan Publishing Company, New York, 1992

[40] L.A. Hayden, J.B. Rettig, "Accuracy and Repeatability in Time Domain Network Analysis," unpublished.

[41] S.P. Lipshitz, R.A. Wannamaker, J. Vanderkooy, "Quantization and Dither: A Theoretical Survey," - *Journal of Audio Engineering Society*, Vol. 40, No. 5, May 1992, pp. 355-375

[42] M.F. Wagdy, "Effect of Various Dither Form on Quantization Errors of Ideal A/D Converters," - *IEEE Transactions on Instrumentation and Measurement*, - Vol. 38, No. 4, August 1989, pp. 850-855

[43] J. B. Rettig, L. Dobos, "Advancement in Picosecond Resolution Time Interval Measurements Techniques," - *Proceedings of the Conference on Precision Electromagnetic Measurements*, Boulder, CO, June 1994

[44] J. Verspecht, "Accurate Spectral Estimation Based on Measurements With a Distorted-Timebase Digitizer," - International Metrology and Test Conference, Irvine, CA, 1993, pp. 699-704

[45] *Understanding Dynamic Range in Transmission Measurements*, Hewlett Packard, May 1988

[46] *Wiltron Product Catalog*, 1992

[47] P.M. Embree, B. Kimble, *C Language Algorithms for Digital Signal Processing*, - Prentice Hall, New Jersey, 1991

[48] D.F. Williams, R.B. Marks, "Accurate Transmission Line Characterization," - *IEEE Microwave and Guided Wave Letters*, Vol. 3, No. 8, August 1993, pp. 247-249

[49] W.L. Gans, "Dynamic Calibration of Waveform Recorders and Oscilloscopes Using Pulse Standards," - *IEEE Transactions on Instrumentation and Measurement*, Vol. 39, No. 6, December 1990, pp. 952-957

[50] A. Bennia, S.M. Riad, "An Optimization Technique for Iterative Frequency-Domain Deconvolution," - *IEEE Transactions on Instrumentation and Measurement*, Vol. 39, No. 2, April 1990, pp. 358-362

[51] A. Bennia, N.S. Nahman, "Deconvolution of Causal Pulse and Transient Data," - *IEEE Transactions on Instrumentation and Measurement*, Vol. 39, No. 6, December 1990, pp. 933-939

APPENDICES

Appendix A. Multiple Reflections in the Device Under Test

If the DUT has complex impedance structure, multiple reflections occur and superpose with each other, causing the TDR/T trace to lose its resolution. The following lattice diagram illustrates this statement.

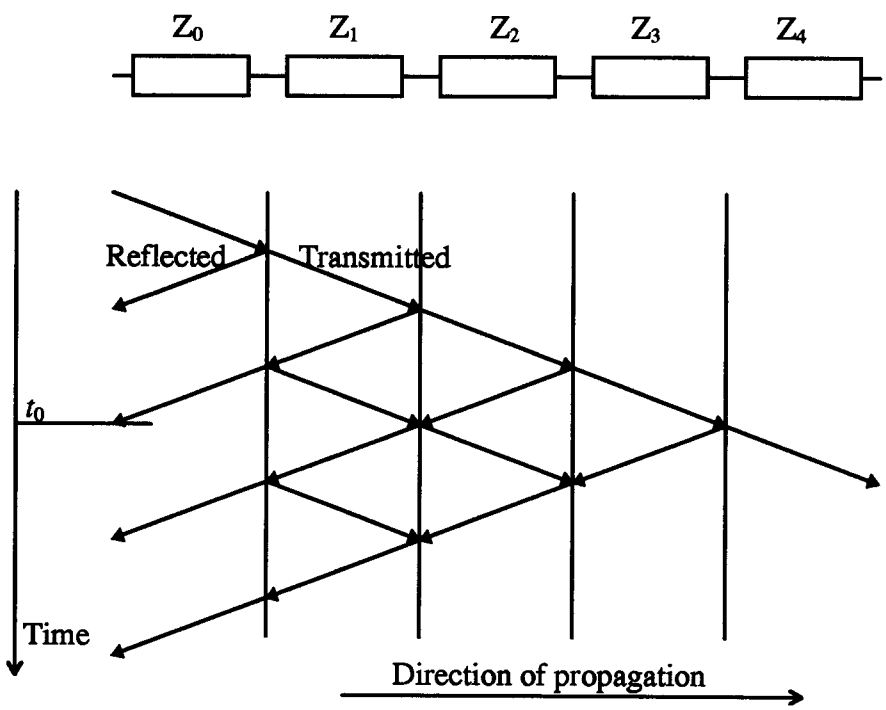

Fig. 22. Lattice diagram of the TDR signal propagating through a complex impedance structure. At the moment t_0 several reflections superpose on each other making it impossible to discern the impedance profile of the structure

At the time t_0 the signal at the receiver will be described by the equation

$$X_{received} = X_{stimulus} \cdot (\Gamma_{01} + T_{01} \cdot \Gamma_{12} \cdot T_{10}) \quad (18)$$

where $X_{received}$ is the received signal, $X_{stimulus}$ is the stimulus signal, Γ_{ij} is the reflection and T_{ij} transmission coefficient at the interface between i and j impedances. The total reflection and transmission measured with the TDR/T system includes all the internal reflections from various discontinuities. Therefore, a deconvolution or peeling algorithm is required to obtain the impedance profile for the DUT, which accounts for all these internal reflections.

Appendix B. An Open-Short-Load-Thru (OSLT) Calibration Procedure

In the OSL calibration approach, the known terminations, which are used to determine the error box coefficients, are open, short and 50 Ω load. Ideal $Z_{short} = 0, \Gamma_{short} = -1$ and $Z_{open} = \infty$, $\Gamma_{open} = 1$, where Z is the corresponding impedance and Γ is the reflection coefficient. Substituting the values for the known calibration standards into the equation for the measured reflection coefficient, we get

$$\Gamma_{M\,load} = \varepsilon_{00} \tag{19}$$

$$\Gamma_{M\,short} = \varepsilon_{00} + \frac{\varepsilon_{10}\varepsilon_{01}}{1+\varepsilon_{11}} \tag{20}$$

$$\Gamma_{M\,open} = \varepsilon_{00} + \frac{\varepsilon_{10}\varepsilon_{01}}{1-\varepsilon_{11}} \tag{21}$$

where *M* stands for "measured." There are an offset for short and for open calibration standards, however, as well as parasitic capacitance of the open. Therefore we need to recalculate Z_{short} and Z_{open} as the impedance at the end of the line using equations (22), (26):

$$Z_{end\,short} = jZ_0 \tan(2\pi f l_{short}) \tag{22}$$

$$Z_{end\,open} = Z_0 \frac{Z_{cap}\cos(2\pi f l_{open}) + jZ_0 \sin(2\pi f l_{open})}{Z_0 \cos(2\pi f l_{open}) + jZ_{cap} \sin(2\pi f l_{open})} \tag{23}$$

$$Z_{cap} = \frac{1}{2\pi f (C_0 + C_1 \cdot f + C_2 \cdot f^2 + C_3 \cdot f^3)},\ Z_0 = 50\,\Omega \tag{24}$$

where f is the frequency. The constants l_{short}, l_{open}, C_0, C_1, C_2, C_3, characterize a model for the short and open for a specific calibration kit and can be found from the calibration kit manuals.

Then the calculated reflection coefficients can be obtained from

$$\Gamma = \frac{Z_{end} - Z_0}{Z_{end} + Z_0} \tag{25}$$

which leads to

$$\Gamma_{short} = -\exp\left(-2j(2\pi f l_{short})\right) \tag{26}$$

and

$$\Gamma_{open} = \exp\left(-2j\beta_{capacitance}\right)\exp\left(-2j(2\pi f l_{open})\right) \tag{27}$$

where $\beta_{capacitance} = \arctan(2\pi f C Z_0)$

Now we can obtain the error coefficients ε_{11} and $\varepsilon_{10}\varepsilon_{01}$ as follows:

$$\varepsilon_{11} = \frac{R-1}{R\cdot\Gamma_{short} - \Gamma_{open}} \tag{28}$$

$$R = \frac{(\Gamma_{M\,short} - \varepsilon_{00})}{(\Gamma_{M\,open} - \varepsilon_{00})}\cdot\frac{\Gamma_{open}}{\Gamma_{short}} \tag{29}$$

$$\varepsilon_{10}\varepsilon_{01} = \frac{\Gamma_{M\,open}}{\Gamma_{open}}\cdot\left(1 - \varepsilon_{11}\cdot\Gamma_{open}\right) \tag{30}$$

The error coefficient ε_{00} is just a frequency domain parameters of the load calibration standard.

Substituting ε_{00}, ε_{00}, $\varepsilon_{10}\varepsilon_{01}$ into equation (31), one can obtain the actual reflection coefficient of DUT:

$$\Gamma_A = \frac{\Gamma_M - \varepsilon_{00}}{\varepsilon_{11} \cdot (\Gamma_M - \varepsilon_{00}) + \varepsilon_{10}\varepsilon_{01}} \tag{31}$$

For the two port measurements the OSLT calibration procedure is used. First, it employs one-port OSL procedure to calibrate each port separately and allows to find ε_{00}, ε_{11} and $\varepsilon_{10}\varepsilon_{01}$ for each port according to equations (19), (28) and (30). Then the measurement ports are connected, directly if possible, and four measurements are taken. These measurements are reflection from the connection between the ports back to the first and the second port ($S_{11\,thru}$, $S_{22\,thru}$), and transmission in both directions ($S_{21\,thru}$, $S_{12\,thru}$).

To calculate the frequency domain parameters for the two-port system, we need to know ε_{22} and $\varepsilon_{10}\varepsilon_{32}$ for each port. They can be found now using the following equations:

$$\varepsilon_{22} = \frac{R}{1 + R \cdot \varepsilon_{11}} \tag{32}$$

$$R = \frac{S_{11\,thru} - \varepsilon_{00}}{\varepsilon_{10}\varepsilon_{01}} \tag{33}$$

$$\varepsilon_{10}\varepsilon_{32} = S_{21\,thru} \cdot (1 - \varepsilon_{11}\varepsilon_{22}) \tag{34}$$

Now the frequency domain parameters for the two port network can be found:

$$S_{11A} = \frac{\left(\frac{S_{11M} - \varepsilon_{00}}{\varepsilon_{10}\varepsilon_{01}}\right)\left(1 + \frac{S_{22M} - \varepsilon'_{33}}{\varepsilon'_{23}\varepsilon'_{32}} \cdot \varepsilon'_{22}\right) - \varepsilon_{22} \cdot \frac{S_{21M}}{\varepsilon_{10}\varepsilon_{32}} \cdot \frac{S_{12M}}{\varepsilon'_{23}\varepsilon'_{01}}}{D} \tag{35}$$

$$S_{21A} = \frac{\frac{S_{21M}}{\varepsilon_{10}\varepsilon_{32}} \cdot \left[1 + \frac{S_{22M} - \varepsilon'_{33}}{\varepsilon'_{23}\varepsilon'_{32}} \cdot (\varepsilon'_{22} - \varepsilon_{22})\right]}{D} \tag{36}$$

$$S_{22A} = \frac{\left(\frac{S_{22M} - \varepsilon'_{33}}{\varepsilon'_{23}\varepsilon'_{32}}\right)\left(1 + \frac{S_{11M} - \varepsilon_{00}}{\varepsilon_{10}\varepsilon_{01}} \cdot \varepsilon_{11}\right) - \varepsilon'_{11} \cdot \frac{S_{21M}}{\varepsilon_{10}\varepsilon_{32}} \cdot \frac{S_{12M}}{\varepsilon'_{23}\varepsilon'_{01}}}{D} \tag{37}$$

$$S_{12A} = \frac{\frac{S_{12M}}{\varepsilon'_{23}\varepsilon'_{01}} \cdot \left[1 + \frac{S_{11M} - \varepsilon_{00}}{\varepsilon_{10}\varepsilon_{01}} \cdot (\varepsilon_{11} - \varepsilon'_{11})\right]}{D} \tag{38}$$

where D can be found as follows:

$$D = \left(1 + \frac{S_{11M} - \varepsilon_{00}}{\varepsilon_{10}\varepsilon_{01}} \cdot \varepsilon_{11}\right)\left(1 + \frac{S_{22M} - \varepsilon'_{33}}{\varepsilon'_{23}\varepsilon'_{32}} \cdot \varepsilon'_{22}\right) - \frac{S_{21M}}{\varepsilon_{10}\varepsilon_{32}} \cdot \frac{S_{12M}}{\varepsilon'_{23}\varepsilon'_{01}} \cdot \varepsilon_{22} \cdot \varepsilon'_{11} \tag{39}$$

Appendix C. Derivation of the Samulon Difference Method

Take the DFT of the finite difference of the original waveform, which is infinite:

$$\begin{aligned} X_{difference}(k) &= \sum_{-\infty}^{\infty}(f_i - f_{i-1})\cdot\exp\left(-j\frac{2\pi ik}{N}\right) \\ &= \sum_{-\infty}^{\infty} f_i\cdot\exp\left(-j\frac{2\pi ik}{N}\right) - \sum_{-\infty}^{\infty} f_{i-1}\cdot\exp\left(-j\frac{2\pi ik}{N}\right) \\ &= \sum_{-\infty}^{\infty} f_i\cdot\exp\left(-j\frac{2\pi ik}{N}\right) - \exp\left(-j\frac{2\pi k}{N}\right)\cdot\sum_{-\infty}^{\infty} f_i\cdot\exp\left(-j\frac{2\pi ik}{N}\right) \\ &= \sum_{-\infty}^{\infty} f_i\cdot\exp\left(-j\frac{2\pi ik}{N}\right)\cdot\left[1-\exp\left(-j\frac{2\pi k}{N}\right)\right] \\ &= X_{original}(k)\cdot\left[1-\exp\left(-j\frac{2\pi k}{N}\right)\right] \end{aligned} \quad (40)$$

Then the spectrum of the original waveform can be recovered using equation

$$X_{original}(k) = \frac{X_{difference}(k)}{1-\exp\left(-j\frac{2\pi k}{N}\right)} \quad (41)$$

Appendix D. Simplifications in the EA-TDR Algorithm

To get the transfer function of the DUT, we need to deconvolve the response of the system from the excitation, or divide the spectrum of the response by the spectrum of the excitation waveform.

$$\begin{aligned} X_{transfer\ function}(k) &= X_{original\ response}(k) \Big/ X_{original\ excitation}(k) \\ &= \frac{X_{difference\ response}(k)}{1-\exp\left(-j\frac{2\pi k}{N}\right)} \Bigg/ \frac{X_{difference\ rexcitation}(k)}{1-\exp\left(-j\frac{2\pi k}{N}\right)} \\ &= X_{difference\ response}(k) \Big/ X_{difference\ excitation}(k) \end{aligned} \tag{42}$$

Therefore, for the further processing purposes, it is possible to substitute the difference waveform spectra for the actual waveform spectra.

Now consider equation (31), describing the one-port error correction procedure. All of the elements in this equation must be transfer functions, with the excitation deconvolved from their spectra. However, it is evident that if we substitute equation (42) in (31), the excitation spectrum will cancel out. Now we will be able to directly substitute the difference waveform spectra for the transfer functions of the DUT and calibration standards.

Appendix E. Different Windowing Function Examples

Examples of the different acquisition window functions, including the Hanning window applied to the 5% of the start and end points in our FFT method, are shown on Fig. 23.

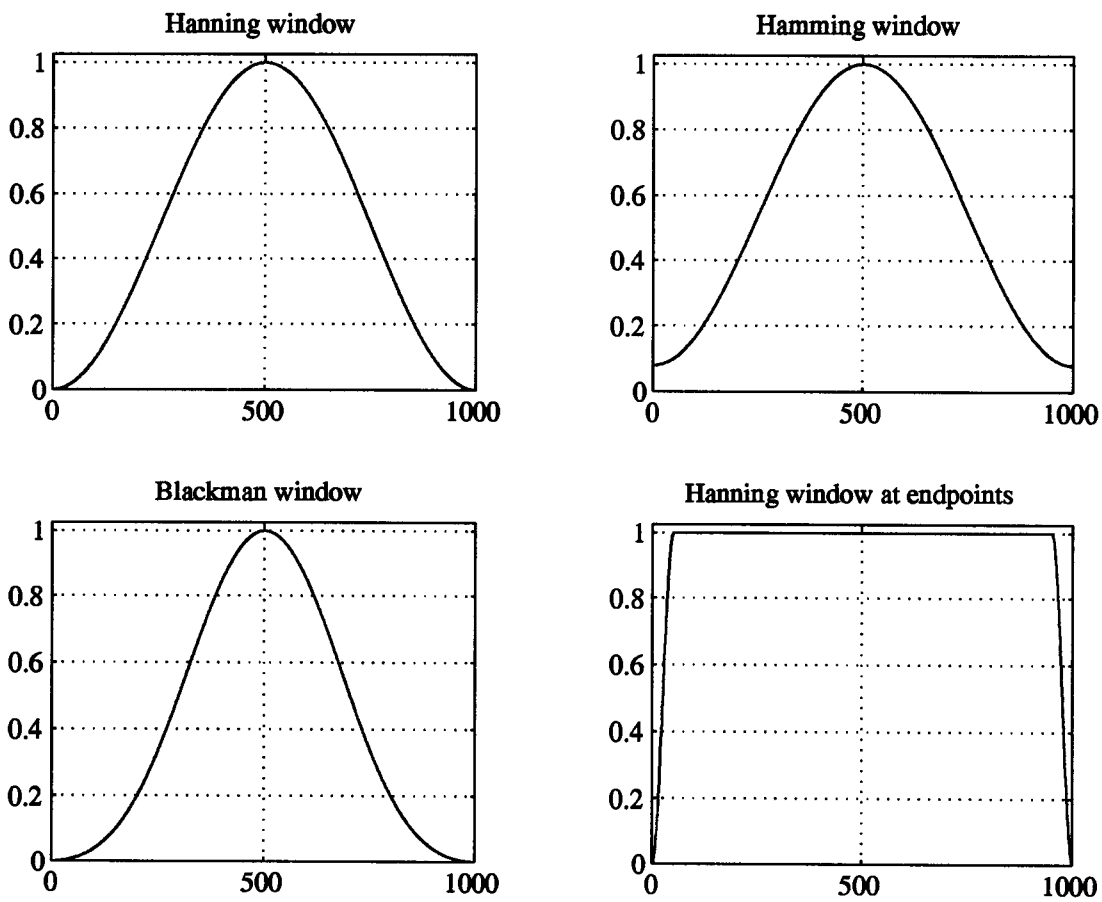

Fig. 23. Different acquisition window function examples

Appendix F. Derivation of the Equation for the System Stimulus Power

It has been shown [33] that Samulon and Gans-Nahman methods for taking the FFT of a step-like waveform are analytically the same. The derivation of equation (10) is more visual for Gans-Nahman method; since both methods are analytically the same, we will derive it for this method only and extend it to the Samulon method.

The Gans-Nahman method is based on turning off the waveform in a "physical" manner. This means that we create a new waveform $f_{physical}$, which is described by the following equation:

$$f_{physical}(k) = f_{original}(k) - f_{original}(k-N)\cdot u(k-N) \tag{43}$$

where $k = 0...2\cdot N-1$, N is the number of points, u(m) is the step function, which means

$$u(m) = \begin{cases} 1, & m \geq 0 \\ 0, & m < 0 \end{cases} \tag{44}$$

In that case the period for our waveform is increased two times, and the new waveform is transformed as shown on the figure below.

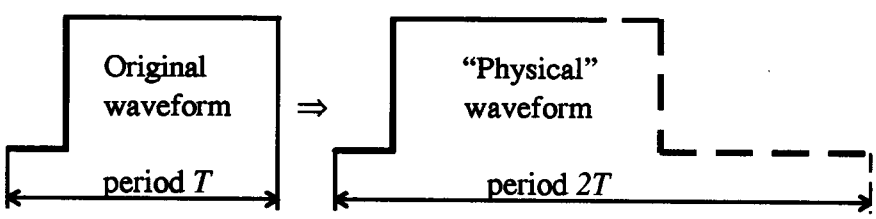

Fig. 24. Gans-Nahman "physical" turning off the waveform

The power is that of a square wave with its length equal half the period of the signal and is

$$P = \left(\frac{2 \cdot A}{\pi \cdot k} \right)^2 \tag{45}$$

where A is the amplitude of the stimulus. Taking into account $k = 2 \cdot f \cdot T$, we get

$$P = \left(\frac{A}{\pi \cdot f \cdot T} \right)^2 \tag{46}$$

Appendix G. Description of Digital Interpolation

Digital interpolation can be performed using *zero-padding* or *zero-packing* and filtering. Both methods assume that the data values outside the acquisition window are the same as the start and end point values. If this condition is met, then the interpolation gives physically correct results.

Zero-padding is a simpler approach. If the start and end points of the data are zeros, we can assume that our data have zero values outside our acquisition window, and add zero values at the start and end of our data, increasing the length of the data by as many times as you want your resolution increased This way we effectively increase our frequency resolution, which is reverse proportional to the length of the acquisition window as described by equation (11). However, zero-padding does not provide a simple way to interpolate the data the FFT of which has already been taken.

Zero-packing and filtering is somewhat more involved. The necessary steps are [47]:

A. Place L-1 zeros between you data samples (the zero-packing step), where L is the factor by which you want to increase the resolution
B. Design a low pass filter capable of attenuating the undesired L-1 spectra above the original spectrum
C. Filter the zero-packed data using the interpolation filter to generate the interpolated data

The zero-packing and filtering approach allows us to deal with the frequency domain data without going back to time domain, thereby providing more flexibility.

Appendix H. Relationship Between the Ideal Step and Pulse Excitations

Consider the following equation:

$$x_{ideal\ step} = \sum_{0}^{N-1} x_{ideal\ pulse} \tag{47}$$

Apply FFT to both sides of equation (47):

$$FFT\left(x_{ideal\ step}\right) = FFT\left(\sum_{0}^{N-1} x_{ideal\ pulse}\right) = \sum_{0}^{N-1} FFT\left(x_{ideal\ pulse}\right) \tag{48}$$

We can get the step response of the system in the same manner: get the pulse response of the system, then sum over all the data to get the step response.

Appendix I. Frequency Domain Network Analysis Measurements

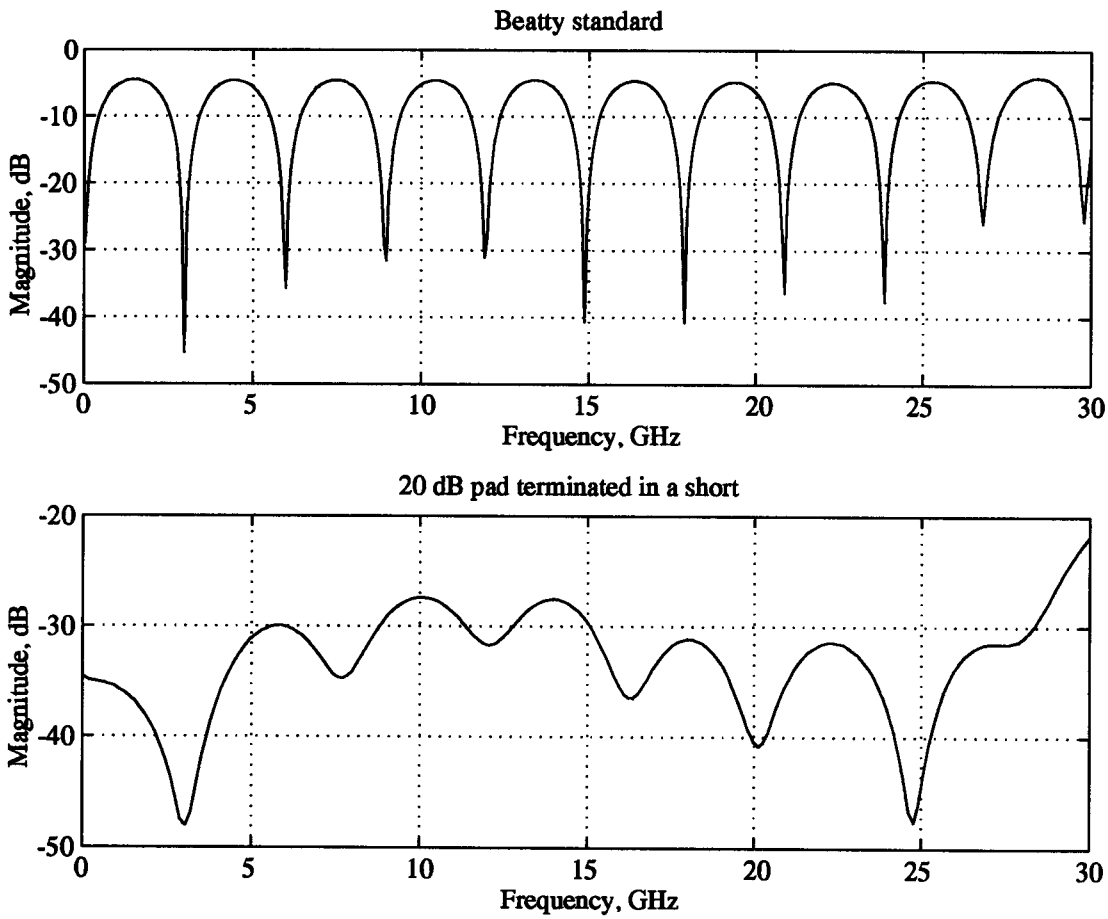

Fig. 25. A Hewlett Packard 8510 vector network analyzer measurement of a Beatty standard (high reflection coefficient) and 20 dB through pad terminated in a short (low reflection coefficient)

Appendix J. Quantization Error Calculation

Tektronix 11801B DSO implements 8 bit voltage (impedance) resolution per vertical scale. There are 10 divisions along the vertical axis of the Tektronix 11801B DSO. The least significant bit will be

$$LSB = \frac{Scale(V/div) \cdot 10\ divisions}{2^b} \tag{49}$$

where b is the number of bits. The quantization error in case of rounding will be half the LSB [29]. The results for LSB and quantization error are summarized in the Table 2.

Table 2. Least significant bit and quantization error for different Tektronix 11801B digital storage oscilloscope settings

Tektronix 11801B DSO Scale (in millivolts per division)	50 mV/div	100 mV/div	200 mV/div
Least Significant Bit	2 mV	4 mV	8 mV
Quantization error	1 mV	2 mV	4 mV